On the Inclusion and Utilization of Pilot Tones in Unique Word OFDM

Christian Hofbauer, *Member, IEEE*, Werner Haselmayr, *Member, IEEE*, Hans-Peter Bernhard, *Senior Member, IEEE*, and Mario Huemer, *Senior Member, IEEE*

Abstract—Unique word-orthogonal frequency division multiplexing (UW-OFDM) is known to provide various performance benefits over conventional OFDM using cyclic prefixes (CP). Most important, UW-OFDM features excellent spectral sidelobe suppression properties and an outstanding bit error ratio performance. Current research has mainly focused on principle performance bounds of UW-OFDM, with less attention on challenges aside from idealized communication scenarios, such as system parameter estimation tasks. In this work we present an approach for including frequency pilots tones into the UW-OFDM signaling scheme, which can then be utilized for these estimation tasks. Suitable optimization criteria are presented and interactions of pilots with data symbols are highlighted. Pilot tone based estimation of a carrier frequency offset (CFO) is conducted as an estimation example, revealing considerable differences to conventional OFDM. Simulation results in a multipath environment demonstrate a significantly increased estimation accuracy in UW-OFDM over CP-OFDM, which becomes even more dominant with an increasing CFO. This performance difference is due to the inherent redundancy present in an UW-OFDM signal.

Index Terms—UW-OFDM, CP-OFDM, unique word, pilot tone, carrier frequency offset

I. INTRODUCTION

The Unique Word (UW)-OFDM signaling scheme introduced in [1] uses a deterministic sequence in the guard interval instead of the conventional cyclic prefix (CP). The introduction of the unique word within the discrete Fourier transform (DFT) interval requires the introduction of redundancy in the frequency domain. This redundancy can advantageously be utilized to provide several beneficial properties, such as superior spectral shaping characteristics [2], [3], [4], [5], [6] or outstanding bit error ratio (BER) performance for linear [7], [8], [2], [9], [10], [11], non-linear [12], [13], [14] as well as iterative [15], [16] receivers[1].

Various other approaches labeled KSP-OFDM (known symbol padding) [19], TDS-OFDM (time domain synchronous) [20], [21], [22], PRP-OFDM (pseudorandom prefix) [23], OFDM with PN (pseudo noise) sequence [22] or even OFDM with UW [24] implement deterministic sequences in the guard

interval. Differing from each other in the specific instance of the sequence, all those schemes implement the guard interval outside of the DFT interval. Hence, no redundancy as in UW-OFDM is present, precluding thus the advantageous properties of UW-OFDM signals.

So far, UW-OFDM has been investigated regarding its principle performance bounds, implying the assumption of several idealized conditions, such as perfect timing, carrier phase or carrier frequency synchronization. The investigation of real-world aspects has been limited to computational complexity analyses [8], [25], peak to average power ratio (PAPR) and peak to minimum power ratio (PMR) considerations [26], [27], as well as the effects of channel estimation errors on the BER performance [2].

One important task in all real-world communication systems is the estimation of various system parameters, which is carried out in time, frequency or both domains. As such, a deterministic time domain sequence like a UW can already offer valuable contributions. However, the domain actually applicable and suitable for a particular estimation problem usually depends on various aspects. These aspects may on the one hand encompass specific requirements of each problem regarding accuracy, computational complexity or real-time constraints, or on the other hand prerequisites like e.g., the underlying signaling scheme. For instance, multicarrier schemes as e.g., OFDM may — due to their inherent structure — prefer utilizing pilot symbols in the frequeny domain (also known as pilot tones) to conduct such system parameter estimation tasks [28].

This work is based on [29] and extends the UW-OFDM concept in order to enable the inclusion of deterministic pilot symbols at dedicated subcarriers in the frequency domain. We therefore provide a generic UW-OFDM signaling framework that enables pilot symbols in both time (i.e., UWs) and frequency domain (i.e., pilot tones). However, the utilization of UWs for actual estimation tasks is beyond the scope of this work[2], and the interested reader is e.g., referred to [19], [22], [23], [30], [31] for details. Instead, we show that due to its specific structure, the UW-OFDM signaling scheme provides a better estimation performance than conventional CP-OFDM, even for an estimator solely based on pilot tones. In this context, we address the following aspects. We investigate the inclusion of pilot tones and study their interaction with data symbol transmission. We introduce suitable cost functions for the optimization of the UW-OFDM transmit signal, identify potential optimization parameters and study their impact on

The authors are with the Silicon Austria Labs GmbH, Linz, Austria (e-mail: {christian.hofbauer, hans-peter.bernhard}@silicon-austria.com), with the Institute of Signal Processing, Johannes Kepler University Linz, Linz, Austria (e-mail: mario.huemer@jku.at), and with the Institute for Communications Engineering and RF-Systems, Johannes Kepler University Linz, Linz, Austria (e-mail: werner.haselmayr@jku.at), respectively.

[1]In this context, the term *iterative receiver* refers to an iterative exchange of realibility (soft) information between detector and decoder [17], [18].

[2]In fact, a utilization of UWs for estimation tasks would limit the comparability with CP-OFDM.

the cost functions. Exemplary generator matrices are presented and their similarities with matrices from pilotless UW-OFDM systems are evaluated. Further, an UW-OFDM signaling model incorporating a carrier frequency offset (CFO) is provided. Moreover, we present a pilot tone based common phase error (CPE) estimation technique, elaborate on the differences to conventional OFDM systems and compare their estimation performance.

We note that this paper expands its conference version [32] in several directions. We describe the generic signaling framework for pilot symbol insertion in more detail. Further, we thoroughly develop the CFO model step-by-step until finally yielding the signaling model presented in [32]. We investigate the approximation error in the signaling model due to partially neglecting intercarrier interference (ICI) and justify its neglection. Moreover, the pilot tone based estimator for the CPE utilized in both works is also explained in more detail, and complemented by an approach to derive the CFO based on the CPE. Finally, the performance of the pilot tone based estimator is evaluated for two different generator matrices instead of only one.

Notation: Vectors and matrices are denoted in bold face lower case $\mathbf{a}$ and upper case letters $\mathbf{A}$, respectively. A tilde is used to explicitly label variables in the frequency domain ($\tilde{\mathbf{a}}$, $\tilde{\mathbf{A}}$). The kth element of a vector $\mathbf{a}$ is named $a[k]$, $[\mathbf{A}]_{k,l}$ addresses the element in column k and row l, $[\mathbf{A}]_{k,*}$ represents all elements of row number k, and $[\mathbf{A}]_{*,l}$ all elements of column number l. The transpose operation is expressed as $(\cdot)^T$, the conjugate transpose or Hermitian as $(\cdot)^H$, expectation as $\mathrm{E}\{\cdot\}$, $\mathrm{tr}(\mathbf{A})$ denotes the trace operation, $\mathrm{diag}(\mathbf{A})$ extracts the main diagonal entries of a matrix $\mathbf{A}$, and $(\cdot)^\dagger$ corresponds to the Moore-Penrose Pseudo-Inverse. The identity matrix is given by $\mathbf{I}$ and a zero matrix as $\mathbf{0}$. A vector $\mathbf{a} \sim \mathcal{CN}(\boldsymbol{\mu}, \mathbf{C})$ denotes a circularly symmetric complex Gaussian noise vector with mean $\boldsymbol{\mu}$ and covariance matrix $\mathbf{C}$. Further, $\hat{\mathbf{a}}$ corresponds to an estimate of $\mathbf{a}$. An underlined letter shall emphasize the motivation behind the specific subscript (or superscript) of $\mathbf{a}_m$. For all signals and systems in this work, the usual equivalent complex baseband representation applies.

The remainder of this paper is organized as follows. Sec. II briefly recaps the UW-OFDM signaling scheme, which is then extended by frequency domain pilot tone insertion in Sec. III. In Sec. IV we investigate the utilization of pilot tones for estimating the CPE and CFO. Subsequently, Sec. V compares the estimation performance in UW-OFDM against CP-OFDM, and Sec. VI finally concludes our work.

II. UW-OFDM SIGNALING SCHEME

The UW-OFDM concept is briefly reviewed in the following, a detailed analytical derivation can be found in [33].

A. Transmit Symbol Generation

Let $\mathbf{x}_u \in \mathbb{C}^{N_u \times 1}$ be a predefined sequence which we call UW. This unique word shall form the tail of each OFDM time domain symbol vector of length N and occupy the guard interval of equal length $N_g = N_u$, as illustrated in Fig. 1. Hence, an OFDM time domain symbol $\mathbf{x}' \in \mathbb{C}^{N \times 1}$ consists of two parts and is of the form $\mathbf{x}' = \begin{bmatrix} \mathbf{x}_{pl}^T & \mathbf{x}_u^T \end{bmatrix}^T$, whereas
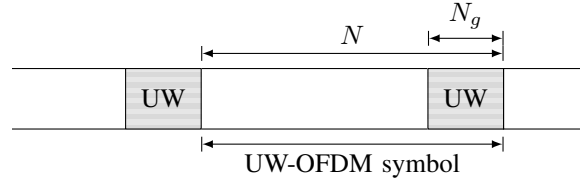

Figure 1: Structure of an UW-OFDM symbol.

$\mathbf{x}_{pl} \in \mathbb{C}^{(N-N_u) \times 1}$ carries the payload affected by the data symbols. Energy arguments elaborated in [33], [34] suggest to first generate an OFDM time domain symbol with a zero-word $\mathbf{x} = \begin{bmatrix} \mathbf{x}_{pl}^T & \mathbf{0}^T \end{bmatrix}^T$, followed by adding the desired UW in time domain in a second step to obtain $\mathbf{x}' = \mathbf{x} + \begin{bmatrix} \mathbf{0}^T & \mathbf{x}_u^T \end{bmatrix}^T$. As in conventional OFDM, unused zero subcarriers together with N_d data symbols $\mathbf{d} \in \mathcal{A}^{N_d \times 1}$ drawn from a symbol alphabet $\mathcal{A}$ shall form an OFDM symbol $\tilde{\mathbf{x}} \in \mathbb{C}^{N \times 1}$ in the frequency domain. Since UW-OFDM additionally demands a zero-word in time domain as part of $\mathbf{x}$, the system of equations $\mathbf{F}_N^{-1} \tilde{\mathbf{x}} = \mathbf{x}$, whereas $\mathbf{F}_N^{-1}$ denotes the inverse DFT of size N with $\mathbf{F}_N^{-1} = \frac{1}{N} \mathbf{F}_N^H$ and $[\mathbf{F}_N]_{k,l} = \mathrm{e}^{-j\frac{2\pi}{N}kl}$, can only be fulfilled by reducing the number of data symbols in the frequency domain by at least N_u, and instead introducing a certain kind of redundancy. For this purpose, let $\mathbf{G} \in \mathbb{C}^{(N_d+N_r) \times N_d}$ be a generator matrix with $N_r = N_u$, which ensures all these requirements. Furthermore, and w.l.o.g., we decompose $\mathbf{G}$ into submatrices according to

$$\mathbf{G} = \mathbf{A} \begin{bmatrix} \mathbf{I} \\ \mathbf{T} \end{bmatrix} \qquad (1)$$

to distinctly address the different requirements on $\mathbf{G}$. Hence, this leads to the time-frequency relation

$$\mathbf{x} = \mathbf{F}_N^{-1} \mathbf{B} \mathbf{A} \begin{bmatrix} \mathbf{I} \\ \mathbf{T} \end{bmatrix} \mathbf{d} = \begin{bmatrix} \mathbf{x}_{pl} \\ \mathbf{0} \end{bmatrix}. \qquad (2)$$

Independent of $\mathbf{G}$, matrix $\mathbf{B} \in \{0,1\}^{N \times (N_d+N_r)}$ models the insertion of optional N_z zero subcarriers for spectral shaping reasons, completing the total number of subcarriers of $N = N_d + N_r + N_z$.

Within $\mathbf{G}$, the identity matrix $\mathbf{I}$ takes care of mapping the data symbols onto $\mathbf{x}$. Further, $\mathbf{T}$ automatically generates the desired zero-word in time domain by simply choosing $\mathbf{T} = -(\mathbf{M}_{22})^{-1}\mathbf{M}_{21}$, $\mathbf{T} \in \mathbb{C}^{N_r \times N_d}$, with appropriately sized submatrices from $\mathbf{F}_N^{-1} \mathbf{B} \mathbf{A} = \begin{bmatrix} \mathbf{M}_{11} & \mathbf{M}_{12} \\ \mathbf{M}_{21} & \mathbf{M}_{22} \end{bmatrix}$, regardless of the specific realizations of $\mathbf{B}$ and $\mathbf{A}$. Finally, $\mathbf{A} \in \mathbb{C}^{(N_d+N_r) \times (N_d+N_r)}$ provides the degrees of freedom to optimize the UW-OFDM generator matrix towards an appropriate cost function to yield certain desired properties. In other words, the decomposition of $\mathbf{G}$ according to (1) has transformed an originally constrained optimization problem into an unconstrained one, as $\mathbf{T}$ will ensure fulfilling the zero-word constraint for any realization of $\mathbf{A}$. The only restriction on $\mathbf{A}$ is its non-singularity due to the inversion of $\mathbf{M}_{22}$. Based on the specific design of $\mathbf{A}$, different classes of UW-OFDM systems emerge, such as *systematically encoded* or *non-systematically encoded* UW-OFDM [33], resulting in a huge collection of

different systems with each individual providing benefits for a different scenario[3].

B. Receiver

After the transmission over a dispersive channel, a received UW-OFDM symbol in the frequency domain carrying the payload (zero subcarriers are excluded) can be formulated as

$$\tilde{\mathbf{y}}_{pl} = \tilde{\mathbf{H}}\mathbf{G}\mathbf{d} + \tilde{\mathbf{H}}\mathbf{B}^T\tilde{\mathbf{x}}_u + \mathbf{B}^T\mathbf{F}_N\mathbf{n}, \qquad (3)$$

whereas $\tilde{\mathbf{H}} \in \mathbb{C}^{(N_d+N_r)\times(N_d+N_r)}$ denotes a diagonal channel matrix with the sampled channel frequency response on its main diagonal, $\tilde{\mathbf{x}}_u = \mathbf{F}_N\begin{bmatrix}\mathbf{0}^T & \mathbf{x}_u^T\end{bmatrix}^T$ corresponds to the frequency domain version of the UW, and $\mathbf{n} \in \mathbb{C}^{N\times1}$ to a noise vector with $\mathbf{n} \sim \mathcal{CN}\left(\mathbf{0}, \sigma_n^2\mathbf{I}\right)$. Subtracting the UW induced offset according to $\tilde{\mathbf{y}} = \tilde{\mathbf{y}}_{pl} - \tilde{\mathbf{H}}\mathbf{B}^T\tilde{\mathbf{x}}_u$ (assuming that the channel matrix $\tilde{\mathbf{H}}$ or at least an estimate of it is available) yields the linear model

$$\tilde{\mathbf{y}} = \tilde{\mathbf{H}}\mathbf{G}\mathbf{d} + \mathbf{v}, \qquad (4)$$

with a noise vector $\mathbf{v} = \mathbf{B}^T\mathbf{F}_N\mathbf{n}$, $\mathbf{v} \sim \mathcal{CN}\left(\mathbf{0}, N\sigma_n^2\mathbf{I}\right)$. One possibility to obtain a data estimate is to apply a linear minimum mean square error (LMMSE) estimator

$$\hat{\mathbf{d}} = (\mathbf{G}^H\tilde{\mathbf{H}}^H\tilde{\mathbf{H}}\mathbf{G} + \tfrac{N\sigma_n^2}{\sigma_d^2}\mathbf{I})^{-1}\mathbf{G}^H\tilde{\mathbf{H}}^H\tilde{\mathbf{y}}, \qquad (5)$$

given a zero-mean data vector with covariance matrix $\sigma_d^2\mathbf{I}$. The covariance matrix of the error $\mathbf{e} = \mathbf{d} - \hat{\mathbf{d}}$ is then

$$\mathbf{C}_{ee} = \mathrm{E}\left\{\mathbf{e}\mathbf{e}^H\right\} = N\sigma_n^2(\mathbf{G}^H\tilde{\mathbf{H}}^H\tilde{\mathbf{H}}\mathbf{G} + \tfrac{N\sigma_n^2}{\sigma_d^2}\mathbf{I})^{-1}. \qquad (6)$$

III. INCLUSION OF PILOT TONES IN UW-OFDM

In this section the UW-OFDM signaling scheme is extended to allow the inclusion of deterministic pilot symbols $\mathbf{p} \in \mathbb{C}^{N_p\times1}$ at dedicated subcarriers in the frequency domain. The presented framework is based on partitioning the signal $\mathbf{x}$ into two additive terms. The first term maps the data symbols on $\mathbf{x}$ by using a generator matrix $\mathbf{G}_d \in \mathbb{C}^{(N_d+N_r+N_p)\times N_d}$, and the second term incorporates the pilot symbols by using $\mathbf{G}_p \in \mathbb{C}^{(N_d+N_r+N_p)\times N_p}$, yielding

$$\mathbf{x} = \mathbf{F}_N^{-1}\mathbf{B}\mathbf{G}_d\mathbf{d} + \mathbf{F}_N^{-1}\mathbf{B}\mathbf{G}_p\mathbf{p} = \begin{bmatrix}\mathbf{x}_d \\ \mathbf{0}\end{bmatrix}. \qquad (7)$$

Matrix $\mathbf{B} \in \mathbb{C}^{N\times(N_d+N_r+N_p)}$ models the insertion of optional zero subcarriers and exactly coincides with matrix $\mathbf{B}$ from the pilotless case in Sec. II-A[4].

The partitioning of the transmit signal in (7) into two additive and independent terms suggests that these two terms can be optimized independently from each other as part of two distinct optimization problems with distinct cost functions. These problems will be tackled in the following.

---

[3]Due to space limitations, the different kinds of generator matrices are not detailed further, instead, the interested reader is referred to [29] for a detailed discussion.

[4]Note that $\mathbf{B}$ is identical for the pilot based and the pilotless case, but the definition of the dimensions differ due to the additional parameter N_p. Contrary to Sec. II-A, it now holds that $N - N_z = N_d + N_r + N_p$ instead of $N - N_z = N_d + N_r$.

A. Optimization of Data Dependent Term

The optimization of the data dependent term can be formulated as an optimization problem for $\mathbf{G}_d$ given as

$$\breve{\mathbf{G}}_d = \underset{\mathbf{G}_d}{\mathrm{argmin}}\left\{J_d\right\} \quad \text{s.t. } \mathbf{F}_N^{-1}\mathbf{B}\mathbf{G}_d = \begin{bmatrix}\mathbf{\Xi} \\ \mathbf{0}\end{bmatrix}, \qquad (8)$$

with J_d denoting an appropriate cost function and $\mathbf{\Xi} \in \mathbb{R}^{N\times(N-N_u)}$ an arbitrary matrix. Similar to the previous section, let us choose the approach

$$\mathbf{G}_d = \mathbf{B}_p\mathbf{A}_d\begin{bmatrix}\mathbf{I} \\ \mathbf{T}_d\end{bmatrix}, \qquad (9)$$

whereas $\mathbf{A}_d \in \mathbb{R}^{(N_d+N_r)\times(N_d+N_r)}$, $\mathbf{B}_p \in \mathbb{C}^{(N_d+N_r+N_p)\times(N_d+N_r)}$, and $\mathbf{T}_d \in \mathbb{C}^{N_r\times N_d}$ with $\mathbf{T}_d = \mathbf{M}_{22}'^{-1}\mathbf{M}_{21}'$. Matrix $\mathbf{B}_p$ places zeros at the positions of the N_p pilot subcarriers and therefore ensures that the data part $\breve{\mathbf{G}}_d\mathbf{d}$ in (7) will not be spread onto the pilot subcarriers. In contrast, however, the pilot part with $\mathbf{G}_p\mathbf{p}$ will overlay the data part to some extent to fulfill the zero word constraint, which will be discussed later on in Sec. III-B. The submatrices $\mathbf{M}_{21}' \in \mathbb{C}^{N_u\times N_d}$ and $\mathbf{M}_{22}' \in \mathbb{C}^{N_u\times N_r}$ with $N_r = N_u$ follow from $\mathbf{F}_N^{-1}\mathbf{B}\mathbf{B}_p\mathbf{A}_d = \begin{bmatrix}\mathbf{M}_{11}' & \mathbf{M}_{12}' \\ \mathbf{M}_{21}' & \mathbf{M}_{22}'\end{bmatrix}$. For pilotless UW-OFDM systems, minimizing the sum of the error covariances after data estimation at a fixed SNR turned out to be a well-chosen cost function J_d for finding generator matrices. In [2] we showed that setting up J_d assuming AWGN conditions with $\mathbf{H} = \mathbf{I}$, an approach to yield an independence of $\mathbf{G}_d$ from dedicated channel realizations, delivers instances of $\mathbf{G}_d$ that feature an outstanding BER performance compared to conventional OFDM. This is especially true for frequency-selective channels, which is particularly astonishing due to the opimization towards an AWGN and thus frequency-flat channel. Therefore, this motivates to apply the same optimization criterion in case of UW-OFDM symbols with pilot subcarriers. Considering (7), the transmit signal $\mathbf{x}''$ can be modelled as

$$\mathbf{x}'' = \mathbf{F}_N^{-1}\left(\mathbf{B}\mathbf{G}_d\mathbf{d} + \mathbf{B}\mathbf{G}_p\mathbf{p} + \tilde{\mathbf{x}}_u\right). \qquad (10)$$

Similar to (3), the frequency domain signal at the receiver (the zero subcarriers are already excluded) can be expressed as

$$\tilde{\mathbf{y}}_{pl} = \tilde{\mathbf{H}}\mathbf{G}_d\mathbf{d} + \tilde{\mathbf{H}}\mathbf{G}_p\mathbf{p} + \tilde{\mathbf{H}}\mathbf{B}^T\tilde{\mathbf{x}}_u + \mathbf{B}^T\mathbf{F}_N\mathbf{n}. \qquad (11)$$

Then, the known signal parts (assuming that $\tilde{\mathbf{H}}$ or at least an estimate of it is available) caused by the UW and the pilots are subtracted from $\tilde{\mathbf{y}}_{pl}$, yielding the linear model

$$\tilde{\mathbf{y}} = \tilde{\mathbf{y}}_{pl} - \tilde{\mathbf{H}}\mathbf{B}^T\tilde{\mathbf{x}}_u - \tilde{\mathbf{H}}\mathbf{G}_p\mathbf{p} \qquad (12)$$

$$= \tilde{\mathbf{H}}\mathbf{G}_d\mathbf{d} + \mathbf{v}. \qquad (13)$$

Putting differences in dimensionality and actual realizations of the involved terms aside, the principle structure of a linear model is the same as in (4). We thus conclude that every UW-OFDM approach — regardless of the presence of pilot symbols in the frequency domain — leads to the same basic transmission model. The main difference between an UW-OFDM system with and without pilot tones is an additional subtraction of the pilot induced offset on top of the UW part to yield the linear model. Based on (13), the following conclusions can be drawn:

- The same structure of a linear transmission model for data symbols enables the deployment of the same estimator concepts as in the case without pilots.
- The same structure of a linear model permits the same optimization procedure as in the pilotless case, which means the same cost function J_d, as well as the same tools to solve the optimization problem in (8). As a consequence, the steepest descent algorithm from [2] developed for the pilotless case can be utilized without adaptations.
- Pilots are introduced for system parameter estimation purposes and then simply subtracted before the data estimation process, as they do not contribute any information to the latter. In this sense, the pilot dependent part can be designed independently from the data dependent part, which is discussed in detail in Sec. III-B.

Fig. 2 illustrates two exemplary generator matrices obtained from solving the optimization problem in (8) for the setup given in Tab. II. These matrices — referred to as $\mathbf{G}'_d$ and $\mathbf{G}''_d$ — are the result of applying the steepest descent algorithm, initialized once with a permutation matrix $\mathbf{P}$ (derived from $\mathcal{I}_r$ in Tab. II) yielding $\mathbf{A}^{(0)} = \mathbf{P}$, and once with $\left[\mathbf{A}^{(0)}\right]_{ij} \sim \mathcal{N}(0,1)$, respectively. The same initialization approaches have been used for the pilotless case. Clearly, the similarities with $\mathbf{G}'$ and $\mathbf{G}''$ from the pilotless case in [2] are immediately apparent, only the setup differs slightly due to the additional N_p pilot subcarriers. $\mathbf{G}'_d$ maps, analogeously to $\mathbf{G}'$, a symbol mainly onto one subcarrier, thus behaving much like a conventional OFDM system, which maps a symbol exclusively on one dedicated subcarrier. $\mathbf{G}''_d$, on the other hand, coincides with $\mathbf{G}''$ in spreading a symbol almost uniformly over all subcarriers, thus appearing similar to a single-carrier based system, which spreads it exactly uniformly over the available bandwidth.

### B. Optimization of Pilot Dependent Term

The pilot symbols $\mathbf{p}$ can usually be freely chosen at design time. Therefore, the pilot dependent term offers an additional degree of freedom besides the generator matrix $\mathbf{G}_p$, leading to the optimization problem

$$\breve{\mathbf{G}}_p, \breve{\mathbf{p}} = \underset{\mathbf{G}_p, \mathbf{p}}{\operatorname{argmin}} \{J_p\} \text{ s.t. } \mathbf{F}_N^{-1}\mathbf{B}\mathbf{G}_p = \begin{bmatrix} \mathbf{\Xi} \\ \mathbf{0} \end{bmatrix} \wedge |p[i]| = 1,$$

(14)

with J_p denoting an appropriate cost function, $\mathbf{\Xi} \in \mathbb{R}^{N \times (N-N_u)}$ again an arbitrary matrix, and $|p[i]| = 1$ with $i = 0, \ldots, N_p - 1$ a constant energy constraint on each individual pilot symbol. In fact, this optimization problem shows strong similarities with the one for finding generator matrices of a systematically encoded UW-OFDM system [33]. Consequently, let us choose the approach

$$\mathbf{G}_p = \mathbf{P}_p \begin{bmatrix} \mathbf{I} \\ \mathbf{T}_p \end{bmatrix},$$

(15)

whereas $\mathbf{I}$ in combination with a permutation matrix $\mathbf{P}_p \in \{0,1\}^{(N_d+N_r+N_p) \times (N_d+N_r+N_p)}$ places the pilot symbols at the corresponding subcarrier positions, and $\mathbf{T}_p \in \mathbb{C}^{(N_d+N_r) \times N_p}$ again ensures the zero-word constraint. Although N_r subcarriers (assuming $N_r = N_u$) would be
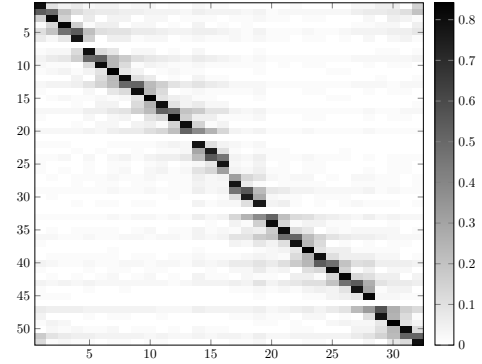
(a) $|\mathbf{G}'_d|$
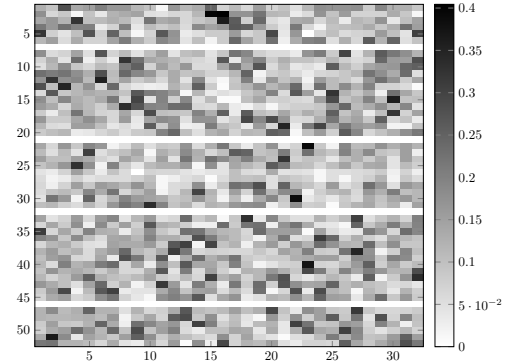
(b) $|\mathbf{G}''_d|$

Figure 2: Magnitude of entries of data generator matrices $\mathbf{G}_d$ based on the setup in Tab. II.

sufficient to fulfill the zero-word constraint from a mathematical point of view (compare with its counterpart $\mathbf{T}_d$ from Sec. III-A), $\mathbf{T}_p$ spreads the required redundancy over $(N_d + N_r)$ subcarriers instead, thus providing additional N_d degrees of freedom in the design of the generator matrix. The matrix $\mathbf{T}_p$ is calculated as $\mathbf{T}_p = -\mathbf{M}_{22}''^{\dagger}\mathbf{M}_{21}''$ with the submatrices $\mathbf{M}_{21}'' \in \mathbb{C}^{N_u \times N_p}$ and $\mathbf{M}_{22}'' \in \mathbb{C}^{N_u \times (N_d+N_r)}$, $N_r = N_u$, derived from $\mathbf{F}_N^{-1}\mathbf{B}\mathbf{P}_p = \begin{bmatrix} \mathbf{M}_{11}'' & \mathbf{M}_{12}'' \\ \mathbf{M}_{21}'' & \mathbf{M}_{22}'' \end{bmatrix}$. Fig. 3 depicts an exemplary generator matrix $\mathbf{G}_p$. As intended, $\mathbf{G}_p$ fulfills its purpose and places the pilot symbols on the designated subcarriers. However, $\mathbf{G}_p$ has to ensure the zero-word constraint at the same time, which is only possible by also spreading (minor) portions of $\mathbf{p}$ on other subcarriers (as already mentioned on at least $N_r = N_u$). To keep spreading at a minimum as there is no other purpose beyond fulfilling the zero-word constraint, a reasonable cost function J_p in (14) is one that delivers $\mathbf{G}_p$ and $\mathbf{p}$ which induce minimum energy[5]. The energy E_p induced by the pilots is given by the cost function[6]

$$J_p = E_p N = \mathbf{p}^H \mathbf{G}_p^H \mathbf{G}_p \mathbf{p}.$$

(16)

The two different factors influencing the resulting energy of the pilots are the positions of the pilot subcarriers determined

---

[5]In this context, spreading redundancy by $\mathbf{T}_p$ on $(N_d + N_r)$ instead of N_r subcarriers helps reducing the required energy J_p.

[6]The energy is scaled by N, originating from the DFT, to easier link the resulting energies with the number of pilots N_p in the subsequent paragraphs.
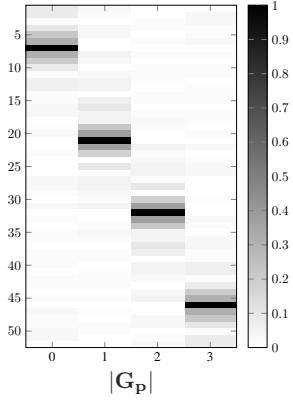
Figure 3: Magnitude of entries of pilot generator matrix $\mathbf{G}_p$ based on the setup in Tab. II.

by $\mathbf{P}_p$ within $\mathbf{G}_p$, and the values of the pilot symbols $\mathbf{p}$. Since it has been shown in [35] that a uniform distribution of the pilot subcarriers over the available bandwidth is beneficial, we fix the position of the pilots accordingly. Hence, the positions are not available as a degree of freedom to minimize (16). In other words, the design of $\mathbf{G}_p$ is fixed and there is no possibility left for optimization of the generator matrix, leaving the values of the pilot symbols $\mathbf{p}$ as only optimization parameters. The original optimization problem in (14) reduces then to

$$\check{\mathbf{p}} = \underset{\mathbf{P}}{\arg\min} \left\{ J_p \right\} \ \wedge \ |p[i]| = 1. \tag{17}$$

The problem can be solved by an exhaustive search, whereas a pilot symbol $p[i]$ is drawn from an alphabet

$$\mathcal{A} = \left\{ e^{j\frac{2\pi\kappa}{|\mathcal{A}|}} \right\} \qquad \kappa = 0 \ldots |\mathcal{A}| - 1 \tag{18}$$

with cardinality $|\mathcal{A}|$, resulting in $|\mathcal{A}|^{N_p}$ different combinations in case of N_p pilot subcarriers. Tab. I shows the corresponding minimum values for E_p as a function of the cardinality of the pilot symbol alphabet, evaluated for a generator matrix $\mathbf{G}_p$ constructed according to the setup parameters in Tab. II and depicted in Fig. 3. For instance, the global minimum energy of 5.1783 in Tab. I follows from evaluating (16) with the pilot symbols $p[i]$ drawn from (18) with $\kappa = k[i]$ and $k[i]$ denoting the ith element of the vector $\mathbf{k} = [17, 14, 3, 0]$. We notice

Table I: Minimum pilot induced energy E_p for an UW-OFDM system with $\mathcal{I}_p = \{7, 21, 43, 57\}$ as pilot subcarrier positions.

$|\mathcal{A}|$	2	4	6	10	20
$N \cdot E_p$	5.4633	5.2423	5.1969	5.1864	5.1783

from Tab. I that the performance does not significantly vary with the cardinality $|\mathcal{A}|$. We conclude that the granularity of the alphabet and thus the optimization effort for the exhaustive search can be kept at a minimum without facing any significant performance loss.

IV. Estimation of Common Phase Error and Carrier Frequency Offset

A well-known critical issue for OFDM systems is the presence of a CFO. A CFO is the result of an oscillator mismatch between transmitter and receiver, or of a Doppler effect due to a movement of at least one of the two. Due to the high sensitivity of OFDM, an accurate estimation and compensation of the CFO is essential. This section will extend the UW-OFDM model in (11) by CFO effects and based on that analyze an estimation algorithm for an CFO induced phase offset. The algorithm is intended to be utilized within the tracking phase [28] of an overall CFO estimation and compensation task and shall take over a fine CFO estimation on an OFDM symbol by symbol basis. Due to an aquisition phase normally preceding the tracking, a CFO can safely be assumed to be in the range of a fraction of the subcarrier spacing. In practice, the remaining CFO will be less than 10 % when set in relation to the subcarrier spacing [28]. The CFO effects in this section are detailed up to the level necessary for developing the estimation algorithm in Sec. IV-C. The interested reader is therefore referred to App. A for details on the definitions and derivations.

A. Receiver Model

Assuming a relative[7] carrier frequency offset ϵ, the receive signal of the lth OFDM symbol in the frequency domain incorporating the CFO effects can be modelled by

$$\tilde{\mathbf{y}}_{pl}^{(l)} \approx \tilde{\mathbf{\Lambda}}^{(l)} \tilde{\mathbf{H}} \mathbf{G}_p \mathbf{p} + \tilde{\mathbf{\Lambda}}^{(l)} \tilde{\mathbf{H}} \mathbf{G}_d \mathbf{d}^{(l)} + \tilde{\mathbf{\Lambda}}^{(l)} \tilde{\mathbf{H}} \mathbf{B}^T \tilde{\mathbf{x}}_u + \mathbf{v}, \tag{19}$$

with a minor approximation error that will be investigated in detail in Sec. IV-B. A CFO in the frequency domain modelled by $\tilde{\mathbf{\Lambda}}^{(l)}$ causes three effects on a subcarrier symbol, which can be explained by the decomposition

$$\tilde{\mathbf{\Lambda}}^{(l)} = e^{j\varphi_l} \tilde{\mathbf{\Lambda}}_{\text{stat}}. \tag{20}$$

First, the lth OFDM symbol is *rotated* by an accumulated phase offset φ_l, which is also referred to as CPE in the literature. The other two CFO effects are incorporated in the static matrix $\tilde{\mathbf{\Lambda}}_{\text{stat}} \in \mathbb{C}^{(N-N_z)\times(N-N_z)}$, which is on the one hand (in the considered CFO range of $\epsilon \leq 0.1$) a negligible scaling of the subcarrier symbols represented by the main diagonal entries of $\tilde{\mathbf{\Lambda}}_{\text{stat}}$ (e.g., 0.98 for $\epsilon = 0.1$), and on the other hand an ICI induced disturbance given by the off-diagonal entries.

A full compensation of the CFO induced effects would require an inversion of $\tilde{\mathbf{\Lambda}}^{(l)}$. However, the most dominant out of the three CFO effects is given by φ_l [28]. Hence, an estimation and compensation of φ_l by derotating with its estimate $\hat{\varphi}_l$ — also known as common phase synchronization — is a sufficient countermeasure against CFO induced disturbances [28]. The estimation of φ_l will be tackled in Sec. IV-C.

B. Evaluation of Approximation Error in Receiver Model

The receiver model in (19) is only an approximation, as it neglects the ICI induced disturbances resulting from those UW spectrum parts that overlay otherwise unused zero subcarriers. As detailed in the Appendix in (96), there would be actually an

---

[7] A relative carrier frequency offset ϵ is defined as $\epsilon = \frac{f_{\text{CFO}}}{\Delta_f}$, whereas f_{CFO} denotes an absolute carrier frequency offset and Δ_f the absolute subcarrier spacing of the system in consideration.

additional fifth term $\tilde{\boldsymbol{\Lambda}}_{zn}^{(l)}\tilde{\mathbf{H}}_z\tilde{\mathbf{x}}_{u,z}$ in (19). This term represents that portion of the UW in frequency domain, which overlays potential z̲ero subcarriers, i.e., $\tilde{\mathbf{x}}_{u,z}$, and is then spread on n̲on-zero subcarriers due to ICI effects modelled within $\tilde{\boldsymbol{\Lambda}}_{zn}^{(l)}$[8]. The following part will investigate the approximation error in (19) in detail and confirm that this error is negligible.

Normally, zero subcarriers follow a dedicated purpose like shaping the spectral mask. Hence, a UW might be chosen and designed already beforehand to explicitly maintain these properties and thus justify our approximation. However, even if this is not possible, one can still simply subtract the corresponding offset, given the availability of an estimate of $\tilde{\boldsymbol{\Lambda}}_{zn}^{(l)}$ and the channel frequency response $\tilde{\mathbf{H}}_z$ on the z̲ero subcarriers. The question remains though, if the effort for estimation and subtraction even translates to any noticeable performance gain, which is investigated next. For that, we elaborate on the error introduced by ICIs in principle in a first step (Fig. 4), and complement this elaboration with practical examples in a second step (Fig. 5).

Overall, the entries of $\tilde{\boldsymbol{\Lambda}}_{zn}^{(l)}$ incorporate the potential impact of ICIs. Fig. 4 plots the magnitude of the entries of the kth row for $\epsilon = 0.1$, which determine the influence of the neighbors on the kth subcarrier due to ICI. Since the magnitudes of
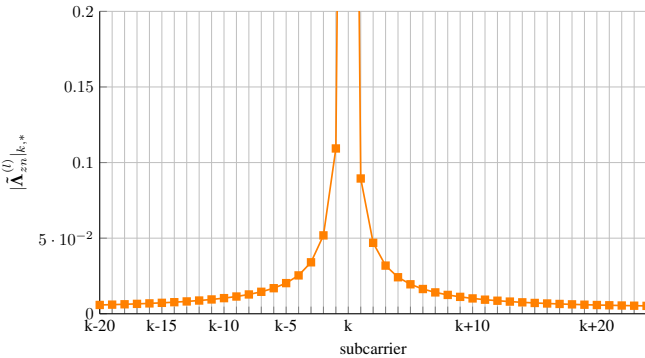

Figure 4: Magnitude of ICI effects experienced by the kth subcarrier from its neighboring subcarriers, with $\epsilon = 0.1$ and $|\tilde{\boldsymbol{\Lambda}}_{zn}^{(l)}|_{k,k} = 0.98$.

the ICI coefficients monotonically increase in ϵ, this denotes the worst-case-scenario for ICI effects seen in the considered tracking phase. Obviously, the impact of ICI declines rapidly as a function of the distance, from 0.1 for the first to already 0.03 for the third neighboring subcarrier. From a practical point of view, this means that independent of the actual UW load on the subcarriers, only the close neighboring subcarriers are likely to cause any relevant ICI induced disturbances. Consequently, these observations already strongly indicate that the approximation error shall always be rather small. In order to complete investigations, Fig. 5 examines the resulting ICI effects evaluated for actual UWs, namely a CAZAC [36], a Barker [37] and the UW sequence from IEEE 802.16 [38]. It depicts for each utilized (i.e., non-zero) subcarrier the ratio

---

[8]Note that $\tilde{\boldsymbol{\Lambda}}_{zn}^{(l)}$ can be decomposed into the same CFO effects as $\tilde{\boldsymbol{\Lambda}}^{(l)}$ in (20).
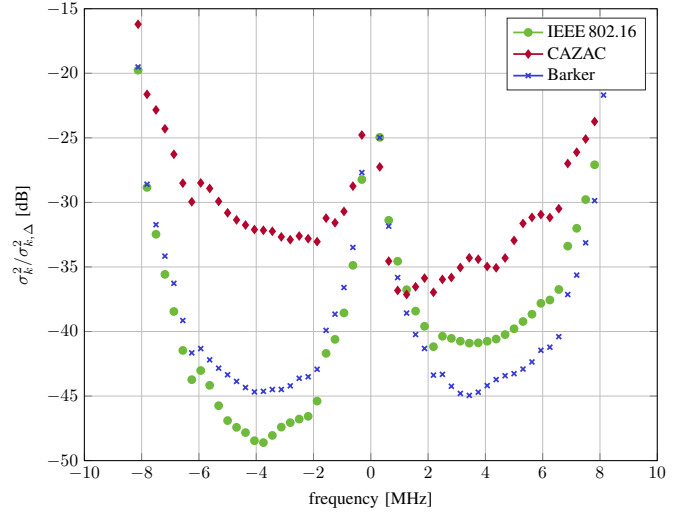

Figure 5: Evaluation of approximation error in (19) due to neglecting ICI induced disturbances from UWs on non-zero subcarriers. Investigated scenario: $\mathbf{G}_d'$, $\mathbf{G}_p$, $\tilde{\mathbf{H}}_p = \mathbf{I}$, $\epsilon = 0.1$ and $\sigma_v^2 = 0$.

between the average power of the approximated signal in (19) with

$$\sigma_k^2 = \mathrm{E}\left\{\tilde{y}_{pl}[k]\tilde{y}_{pl}[k]^H\right\}, \qquad (21)$$

and the average power of the approximation error

$$\sigma_{k,\Delta}^2 = \mathrm{E}\left\{\left[\left(\tilde{\boldsymbol{\Lambda}}_{zn}\tilde{\mathbf{H}}_z\tilde{\mathbf{x}}_{u,z}\right)\left(\tilde{\boldsymbol{\Lambda}}_{zn}\tilde{\mathbf{H}}_z\tilde{\mathbf{x}}_{u,z}\right)^H\right]_{k,k}\right\}, \quad (22)$$

which corresponds to the ICI induced disturbances originating from the UW load on zero subcarriers. It turns out that the impact of an ICI induced UW error is in a negligible range, at most at the edges of the utilized bandwidth it might be in a noticeable range. In conclusion, the approximation error is non-dominant in practical scenarios and therefore justifies the simplification in (19). Hence, in the following investigations the approximate model in (19) can be used.

C. Estimation of CPE φ_l

There are various approaches for estimating the CPE φ_l in OFDM systems, e.g., based on data symbols [39], [40] known as decision directed schemes or cyclic prefix based methods [41], [42]. Another common way is the utilization of pilot symbols $\mathbf{p}$ in the frequency domain [28] to obtain the estimate

$$\hat{\varphi}_l = \arg\left(\mathbf{p}^H\mathbf{W}_p\hat{\mathbf{p}}^{(l)}\right). \qquad (23)$$

The estimate $\hat{\mathbf{p}}^{(l)}$ is attained from the lth received OFDM symbol in (19) and $\mathbf{W}_p = \mathrm{diag}\left(\mathbf{w}_p\right)$ is a diagonal weighting matrix with $\mathbf{w}_p \in \mathbb{R}_+^{0\ (N_p \times 1)}$ to rate the pilots regarding their estimation quality (e.g., based on the inverse main diagonal of an error covariance matrix). In order to evaluate the applicability of this concept to UW-OFDM as well, let us investigate the CFO effects on the pilot symbols in more detail. The general definition of a received OFDM symbol introduced in (19) serves as a starting point to obtain $\hat{\mathbf{p}}^{(l)}$. We apply a linear estimator $\mathbf{E}_p' = \mathbf{E}_p\tilde{\mathbf{H}}^{-1}$ consisting of two

stages. The first stage inverts the channel, and the second stage $\mathbf{E}_p = \begin{bmatrix} \mathbf{I} & \mathbf{0} \end{bmatrix} \mathbf{P}_p^T$ extracts the pilots from the frequency domain vector, with the permutation matrix $\mathbf{P}_p$ from (15). We are aware that $\mathbf{E}_p$ is only suboptimum in terms of estimation performance, as it is not capable of exploiting the portion of the pilots spread on the non-pilot subcarriers due to $\mathbf{G}_p \mathbf{p}$. This for instance would be possible with a best linear unbiased estimator (BLUE) $\mathbf{E}_p = \mathbf{G}_p^\dagger$ [43]. Nevertheless, this suboptimum approach does e.g., not require the subtraction of the data and UW dependent offset term in (19) to transform an affine into a linear model [43], which therefore simplifies the estimation task greatly. Applying $\mathbf{E}_p'$ leads to

$$\hat{\mathbf{p}}^{(l)} = \mathbf{E}_p \tilde{\mathbf{H}}^{-1} \tilde{\mathbf{y}}_{pl}^{(l)} \tag{24}$$

$$= \mathbf{E}_p \tilde{\mathbf{H}}^{-1} \tilde{\mathbf{\Lambda}}^{(l)} \tilde{\mathbf{H}} \mathbf{G}_p \mathbf{p} + \mathbf{E}_p \tilde{\mathbf{H}}^{-1} \tilde{\mathbf{\Lambda}}^{(l)} \tilde{\mathbf{H}} \mathbf{G}_d \mathbf{d}^{(l)}$$

$$+ \mathbf{E}_p \tilde{\mathbf{H}}^{-1} \tilde{\mathbf{\Lambda}}^{(l)} \tilde{\mathbf{H}} \mathbf{B}^T \tilde{\mathbf{x}}_u + \mathbf{E}_p \tilde{\mathbf{H}}^{-1} \mathbf{B}^T \mathbf{v} \tag{25}$$

$$= \mathbf{E}_p \tilde{\mathbf{\Lambda}}_h^{(l)} \left(\mathbf{G}_p \mathbf{p} + \mathbf{B}^T \tilde{\mathbf{x}}_u \right) + \mathbf{d}_{\text{ICI}}^{(l)} + \mathbf{v}''. \tag{26}$$

Pilot and data symbols are orthogonal in frequency domain, but $\tilde{\mathbf{\Lambda}}^{(l)}$ introduces intercarrier interference resulting in

$$\mathbf{d}_{\text{ICI}}^{(l)} = \mathbf{E}_p \tilde{\mathbf{H}}^{-1} \tilde{\mathbf{\Lambda}}^{(l)} \tilde{\mathbf{H}} \mathbf{G}_d \mathbf{d}^{(l)}, \tag{27}$$

with $\mathbf{d}_{\text{ICI}}^{(l)} \in \mathbb{C}^{N_p \times 1}$. The vector $\mathbf{v}'' \in \mathbb{C}^{N_p \times 1}$ represents additive noise according to

$$\mathbf{v}'' = \mathbf{E}_p \tilde{\mathbf{H}}^{-1} \mathbf{B}^T \mathbf{v}. \tag{28}$$

Since $\tilde{\mathbf{\Lambda}}^{(l)}$ has entries off the main diagonal and is only approximately a diagonal matrix, multiplying with $\tilde{\mathbf{H}}^{-1}$ cannot fully equalize the channel $\tilde{\mathbf{H}}$, which is incorporated in

$$\tilde{\mathbf{\Lambda}}_h^{(l)} = \tilde{\mathbf{H}}^{-1} \tilde{\mathbf{\Lambda}}^{(l)} \tilde{\mathbf{H}}. \tag{29}$$

For an easier analysis, a *single* pilot symbol is considered in the following, which is given as

$$\hat{p}^{(l)}[k] = [\mathbf{E}_p]_{k,*} \tilde{\mathbf{\Lambda}}_h^{(l)} \left(\mathbf{G}_p \mathbf{p} + \mathbf{B}^T \tilde{\mathbf{x}}_u \right) + d_{\text{ICI}}^{(l)}[k] + v''[k]$$

$$= [\mathbf{E}_p]_{k,*} \tilde{\mathbf{\Lambda}}_h^{(l)} \left([\mathbf{G}_p]_{*,k} p[k] + \mathbf{B}^T \tilde{\mathbf{x}}_u \right) [\mathbf{E}_p]_{k,*} \tilde{\mathbf{\Lambda}}_h^{(l)}$$

$$\times \sum_{m=0, m \neq k}^{N_p-1} [\mathbf{G}_p]_{*,m} p[m] + d_{\text{ICI}}^{(l)}[k] + v''[k]$$

$$= \mathbf{e}_k^T \tilde{\mathbf{\Lambda}}_h^{(l)} \left(\mathbf{g}_k p[k] + \mathbf{B}^T \tilde{\mathbf{x}}_u \right)$$

$$+ \mathbf{e}_k^T \tilde{\mathbf{\Lambda}}_h^{(l)} \sum_{m=0, m \neq k}^{N_p-1} \mathbf{g}_m p[m] + d_{\text{ICI}}^{(l)}[k] + v''[k]$$

$$= \mathbf{e}_k^T \tilde{\mathbf{\Lambda}}_h^{(l)} \left(\mathbf{g}_k p[k] + \mathbf{B}^T \tilde{\mathbf{x}}_u \right) + p_{\text{ICI}}^{(l)}[k] + d_{\text{ICI}}^{(l)}[k] + v''[k], \tag{30}$$

with $\mathbf{e}_k^T = [\mathbf{E}_p]_{k,*}$, $\mathbf{g}_k = [\mathbf{G}_p]_{*,k}$ and $\mathbf{g}_m = [\mathbf{G}_p]_{*,m}$. Consequently, there are four terms influencing $\hat{p}^{(l)}[k]$. The additive noise term $v''[k]$ should not require any further explanation. The term $d_{\text{ICI}}^{(l)}[k]$ models the ICI driven by data symbols and degrades estimation quality in a similar manner as additive noise. The term

$$p_{\text{ICI}}^{(l)}[k] = \mathbf{e}_k^T \tilde{\mathbf{\Lambda}}_h^{(l)} \sum_{m=0, m \neq k}^{N_p-1} \mathbf{g}_m p[m] \tag{31}$$

comprises the ICI induced by the other pilot symbols. Since the pilot symbols are constant, this term leads to a constant estimation error (assuming a fixed CFO ϵ). In any way, the influence of this term is rather limited. This is due to a usually uniform distribution of the pilot symbols over the available spectrum to optimally support system parameter estimation tasks [35], resulting in a distance of several subcarriers among them, cf. Fig. 3. The first term in (30) comprises the actual pilot symbol, an additive offset caused by the UW and a part causing the CPE to be estimated.

Let the last three terms in (30) form a new additive noise term $v'''[k] = p_{\text{ICI}}^{(l)}[k] + d_{\text{ICI}}^{(l)}[k] + v''[k]$, then the estimation of φ_l reads

$$\hat{\varphi}_l = \arg \left(\mathbf{p}^H \mathbf{W}_p \hat{\mathbf{p}}^{(l)} \right) \tag{32}$$

$$= \arg \left(\sum_{k=0}^{N_p-1} p[k]^H w_p[k] \hat{p}^{(l)}[k] \right) \tag{33}$$

$$= \arg \left(\sum_{k=0}^{N_p-1} \mathbf{e}_k^T \tilde{\mathbf{\Lambda}}_h^{(l)} \left(\mathbf{g}_k w_p[k] |p[k]|^2 + \mathbf{B}^T \tilde{\mathbf{x}}_u w_p[k] p[k]^H \right) \right.$$

$$\left. + v'''[k] w_p[k] p[k]^H \right) \tag{34}$$

$$= \arg \left(\underbrace{\sum_{k=0}^{N_p-1} \mathrm{e}^{j\varphi_l} \mathbf{e}_k^T \tilde{\mathbf{\Lambda}}_{h,\text{stat}} w_p[k] \left(\mathbf{g}_k |p[k]|^2 + \mathbf{B}^T \tilde{\mathbf{x}}_u p[k]^H \right)}_{\text{pilot term}} \right.$$

$$\left. + \underbrace{\sum_{k=0}^{N_p-1} v'''[k] w_p[k] p[k]^H}_{\text{noise term}} \right), \tag{35}$$

with $\tilde{\mathbf{\Lambda}}_{h,\text{stat}} = \tilde{\mathbf{H}}^{-1} \tilde{\mathbf{\Lambda}}_{\text{stat}} \tilde{\mathbf{H}}$. The angle $\hat{\varphi}_l$ depends now on two sources, with the first one denoted as *pilot term* and the second one as *noise term*. Through investigation of the individual terms in (35) it can be shown that the noise term has only a minor impact on $\arg(\cdot)$, i.e., (35) almost equals an argument soley taken from the pilot term. This translates to the model

$$\hat{\varphi}_l = \arg \left(\sum_{k=0}^{N_p-1} \mathrm{e}^{j\varphi_l} \mathbf{e}_k^T \tilde{\mathbf{\Lambda}}_{h,\text{stat}} \left(\mathbf{g}_k w_p[k] |p[k]|^2 \right. \right.$$

$$\left. \left. + \mathbf{B}^T \tilde{\mathbf{x}}_u w_p[k] p[k]^H \right) \right) + \Delta_l \tag{36}$$

$$= \arg \left(\mathrm{e}^{j\varphi_l} \sum_{k=0}^{N_p-1} w_p[k] \left(\mathbf{e}_k^T \tilde{\mathbf{\Lambda}}_{h,\text{stat}} \mathbf{g}_k |p[k]|^2 \right. \right.$$

$$\left. \left. + \mathbf{e}_k^T \tilde{\mathbf{\Lambda}}_{h,\text{stat}} \mathbf{B}^T \tilde{\mathbf{x}}_u p[k]^H \right) \right) + \Delta_l, \tag{37}$$

with Δ_l denoting minor additive deviation approximated by

$$\Delta_l \approx f \left(\sum_{k=0}^{N_p-1} v'''[k] w_p[k] p[k]^H \right). \tag{38}$$

We assume $f(\cdot)$ to be a proper function that takes care (in a not further specified way) of shifting the deviation outside

of $\arg(\cdot)$. A detailed specification of the function $f(\cdot)$ is not of relevance for the subsequent analysis and is therefore disregarded. The expression in (37) is still quite complex and requires additional simplification to allow an intuitive interpretation of the impact factors on $\hat{\varphi}_l$. Let us therefore introduce the magnitude and phase representation

$$a_{p,k}e^{j\varphi_{p,k}} = w_p[k]\mathbf{e}_k^T\tilde{\boldsymbol{\Lambda}}_{h,\text{stat}}\left(\mathbf{g}_k|p[k]|^2 + \mathbf{B}^T\tilde{\mathbf{x}}_u p[k]^H\right) \quad (39)$$

$$a_p e^{j\varphi_p} = \sum_{k=0}^{N_p-1} a_{p,k}e^{j\varphi_{p,k}}, \quad (40)$$

then the estimated CPE $\hat{\varphi}_l$ can finally be written as

$$\hat{\varphi}_l = \arg\left(e^{j\varphi_l}\sum_{k=0}^{N_p-1} a_{p,k}e^{j\varphi_{p,k}}\right) + \Delta_l \quad (41)$$

$$= \arg\left(e^{j\varphi_l}a_p e^{j\varphi_p}\right) + \Delta_l \quad (42)$$

$$= \varphi_l + \varphi_p + \Delta_l. \quad (43)$$

We observe that the estimate $\hat{\varphi}_l$ in (43) consists of the true CPE φ_l disturbed by φ_p and Δ_l. While Δ_l occurs in UW-OFDM and CP-OFDM (but with different values), the phase offset φ_p is only present in UW-OFDM. As observable from (39), this is due to a non-zero UW and an additional scaling and rotating of the pilot symbol. The latter originates from the fact that $\mathbf{G}_p$ places a pilot symbol at the dedicated subcarrier position, but also spreads portions of it over the remaining subcarriers to fulfill the zero-word constraint of UW-OFDM, cf. (7). In combination with $\tilde{\boldsymbol{\Lambda}}^{(l)}$, the portions of a pilot symbol spread over several subcarriers are leaked back. This leads to an ICI induced self interference of the pilot symbols, which has to be accounted for. Therefore, we present an approach in the following to compensate the induced phase offset φ_p within the estimate $\hat{\varphi}_l$.

D. Compensation of Phase Offset φ_p in $\hat{\varphi}_l$

The first step towards offset compensation in (43) is now to obtain an estimate of φ_p. There are two problems emerging in this context as a result of the dependence of φ_p on ϵ due to $\tilde{\boldsymbol{\Lambda}}_{h,\text{stat}}$. First and addressed in this section, a straightforward relationship between φ_p and ϵ is not immediately apparent from (39)–(40). Second and addressed subsequently in Sec. IV-E, an estimate $\hat{\varphi}_p$ requires also an estimate $\hat{\epsilon}$, which in turn has to somehow be obtained from $\hat{\varphi}_l$ based on the relationship between φ_l and ϵ (see (88) in the Appendix), thus leading to mutual dependencies among φ_l, φ_p and ϵ.

We have confirmed through empirical investigations that φ_p can be modelled as

$$\varphi_p = m\epsilon + q, \qquad m, q \in \mathbb{R}, \quad (44)$$

in the relevant CFO range of $\epsilon \leq 0.1$. This behavior is exemplarily shown in Fig. 6 for the pilot generator matrix $\mathbf{G}_p$ visualized in Fig. 3 in case of $\tilde{\mathbf{H}}_p = \mathbf{I}$, $\mathbf{W}_p = |\tilde{\mathbf{H}}_p|^2 = \mathbf{I}$ and different UWs. Here, $\tilde{\mathbf{H}}_p \in \mathbb{C}^{N_p \times N_p}$ denotes a diagonal matrix with the channel coefficients corresponding to the pilot subcarriers on the main diagonal. It turns out that for $\tilde{\mathbf{x}}_u \neq \mathbf{0}$, the offset is approximately an affine function of ϵ for the relevant CFO range (i.e., $\epsilon \leq 0.1$) for a given setup,
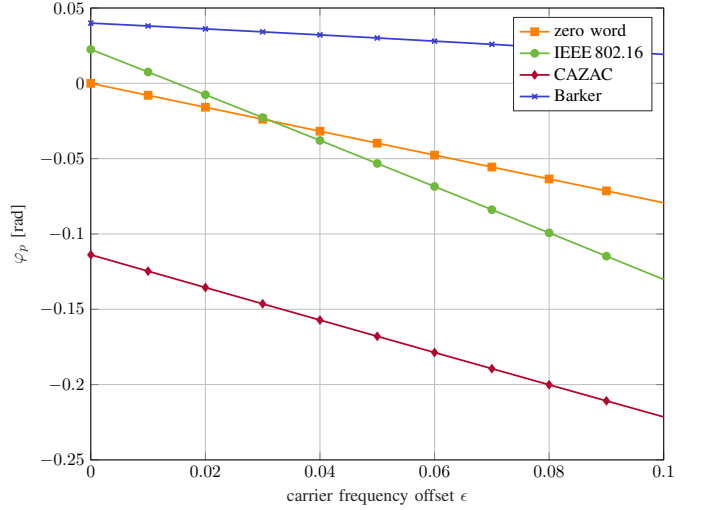

Figure 6: UW-OFDM specific phase offset φ_p for different UWs when estimating the CPE φ_l caused by a CFO. Investigated scenario: $\mathbf{G}_p$, $\tilde{\mathbf{H}}_p = \mathbf{I}$, $\sigma_v^2 = 0$ and $\mathbf{W}_p = \mathbf{I}$.

which collapses to a linear function in case of $\tilde{\mathbf{x}}_u = \mathbf{0}$. In particular, if $\epsilon = 0$, then the matrix $\tilde{\boldsymbol{\Lambda}}_{h,\text{stat}}$ in (39) collapses to an identity matrix for any realization of $\tilde{\mathbf{H}}$, resulting in $\mathbf{e}_k^T\tilde{\boldsymbol{\Lambda}}_{h,\text{stat}}\mathbf{g}_k = 1$ and $\mathbf{e}_k^T\tilde{\boldsymbol{\Lambda}}_{h,\text{stat}}\mathbf{B}^T\tilde{\mathbf{x}}_u = \tilde{x}_u[i_{p,k}]$, with $i_{p,k}$ addressing the kth element of the ordered pilot subcarrier index set $\mathcal{I}_{p,o} = (\mathcal{I}_p, <)$ defined as

$$\mathcal{I}_{p,o} = \left\{i_{p,0}, i_{p,1}, \dots i_{p,N_p-1}\right\}. \quad (45)$$

In this context, an estimate follows then as

$$\hat{\varphi}_{p|\epsilon=0} = q$$

$$= \arg\left(\sum_{k=0}^{N_p-1} w_p[k]\left(|p[k]|^2 + \tilde{x}_u[i_{p,k}]p[k]^H\right)\right) + \Delta_l$$

$$\approx \arg\left(\sum_{k=0}^{N_p-1} w_p[k]\left(|p[k]|^2 + \tilde{x}_u[i_{p,k}]p[k]^H\right)\right). \quad (46)$$

Clearly, the constant phase offset q originates from the presence of a non-zero UW and vanishes in case of $\tilde{\mathbf{x}}_u = \mathbf{0}$ and thus $\tilde{x}_u[i_{p,k}] = 0$. The actual value of q depends on the UW offset at the specific subcarriers and the pilot symbols themselves. Note that the affine model in (44) could easily be transformed into a linear model by the definition of new pilot symbols $\mathbf{p}' = \mathbf{p} + \tilde{\mathbf{x}}_{u,\mathcal{I}_p}$, where $\tilde{\mathbf{x}}_{u,\mathcal{I}_p}$ denotes a vector with elements out of $\tilde{\mathbf{x}}_u$ at the corresponding pilot subcarrier positions. The estimation of φ_l follows then according to $\hat{\varphi}_l = \arg\left(\mathbf{p}'^H\mathbf{W}_p\hat{\mathbf{p}}^{(l)}\right)$.

The variable part $m\epsilon$ within the phase offset model for φ_p exists independent of the presence of a zero or non-zero UW. The slope m is determined by both sources, the UW and the rotation and scaling of the pilot symbols

$$m\epsilon = \arg\left(\sum_{k=0}^{N_p-1} \mathbf{e}_k^T\tilde{\boldsymbol{\Lambda}}_{h,\text{stat}}\mathbf{g}_k w_p[k]|p[k]|^2 \right.$$

$$\left. + \mathbf{e}_k^T\tilde{\boldsymbol{\Lambda}}_{h,\text{stat}}\mathbf{B}^T\tilde{\mathbf{x}}_u w_p[k]p[k]^H\right) - q, \quad (47)$$

which in turn depend on the channel realization $\tilde{\mathbf{H}}$, the generator matrix $\mathbf{G}_p$, the estimator $\mathbf{E}_p$, and the pilot symbols $\mathbf{p}$. Regardless of the specific values of these parameters, the affine model for φ_p as a function of ϵ holds in the relevant range.

In a real communication system, the parameters of the affine model for φ_p in (44) are easily determined. Given a certain setup and assuming knowledge of the channel $\tilde{\mathbf{H}}$ or an estimate of it (which does not induce an additional effort as it is required for other purposes anyway), the parameters can be derived by numerically evaluating φ_p at two different points, e.g., for $\epsilon = 0$ and $\epsilon = 0.1$. Inserting then (44) into (43) yields

$$\hat{\varphi}_l = \varphi_l + \varphi_p + \Delta_l \tag{48}$$
$$= \varphi_l + m\epsilon + q + \Delta_l. \tag{49}$$

Finally, compensating the offset φ_p by its estimate $\hat{\varphi}_p$ delivers a new estimate for the CPE

$$\hat{\hat{\varphi}}_l = \hat{\varphi}_l - \hat{\varphi}_p = \hat{\varphi}_l - m\hat{\epsilon} - q. \tag{50}$$

E. Estimation of CFO ϵ

The presented linearization in (44) highlights the simple relationship between the phase offset φ_p and the CFO ϵ, thus allowing for an easy compensation. In a real system, however, φ_p is not available and we have to obtain an estimate

$$\hat{\varphi}_p = m\hat{\epsilon} + q \tag{51}$$

instead, which in turn requires an estimate $\hat{\epsilon}$. This will be provided next. The obvious way is exploiting the linear relationship between φ_l and the CFO ϵ from (88). In practice, there is only the estimate $\hat{\varphi}_l$ avaible which incorporates the unknown offset φ_p as detailed in (43), thus leading to mutual dependencies. Fortunately, the approximation of φ_p as a linear function of ϵ resolves these dependencies. Introducing the prefactor $\frac{2\pi}{N}\epsilon$ to model $m = N_p \frac{2\pi}{N}\epsilon$ with a constant $N_p \in \mathbb{R}$, and using (88) together with (49) yields

$$\hat{\epsilon}_l = \epsilon + \Delta_{\epsilon_l} \tag{52}$$
$$= (\hat{\varphi}_l - q) \frac{N}{2\pi \left(Nl + N_u + \frac{N-1}{2} + N_p \right)}. \tag{53}$$

The error Δ_{ϵ_l} in $\hat{\epsilon}_l$ decreases with increasing $\hat{\varphi}_l$ due to Nl in the denominator. However, the proposed estimation algorithm $\hat{\varphi}_l = \arg\left(\mathbf{p}^H \mathbf{W}_p \hat{\mathbf{p}}^{(l)} \right)$ implicitly applies a modulo operation on $\hat{\varphi}_l$ over the range $[0, 2\pi)$, whereas the estimator in (53) requires the total angle accumulated from the beginning of the burst up to and including OFDM symbol l. This restriction limits the applicability to angles φ_l not exceeding 2π and thus also the estimation accuracy. One way to circumvent this restriction is averaging over several estimates $\hat{\epsilon}_l$, gained from the knowledge that the angle increases linearly with

$$\varphi_\Delta = \varphi_l - \varphi_{l-1} = \frac{2\pi}{N}\epsilon \left(Nl - N(l-1) \right) = 2\pi\epsilon \tag{54}$$

between two OFDM symbols. Furthermore, the latter approach offers the advantage of automatically cancelling out the offset $\hat{\varphi}_p$ within φ_Δ.

At this point, let us briefly summarize the presented algorithm for CFO compensation. The most critical CFO effect is

known as CPE, which can be estimated as shown in Sec. IV-C. However, in case of UW-OFDM, this estimate requires a compensation of the incorporated phase offset φ_p. Fortunately, this phase offset can easily be compensated by approximating it as an affine function of ϵ as detailed in Sec. IV-D. This approximation requires in turn an estimate $\hat{\epsilon}$, which can be obtained as shown in Sec. IV-E.

V. Performance Evaluation

The preceding analysis has unveiled a few differences in pilot based CFO estimation between UW-OFDM and CP-OFDM. The question remains, whether these differences have an impact on the estimation quality, which is discussed next.

A. Simulation Setup

Tab. II summarizes the most important setup parameters of the UW-OFDM and CP-OFDM systems in consideration. In order to provide a fair comparison with CP-OFDM, the utilized non-systematically encoded UW-OFDM generator matrices are scaled such that $\mathbf{G}_d^H \mathbf{G}_d = \alpha\mathbf{I}$ with $\alpha = N_d'/N_d$, whereas N_d' denotes the number of data subcarriers of the reference CP-OFDM system. This ensures that the data induced mean power per non-pilot subcarrier is the same for both systems; an important aspect, as this defines the severity of the disturbance caused by $\mathbf{d}_{\text{ICI}}^{(l)}$, cf. (26). This is even slightly advantageous for CP-OFDM, since in UW-OFDM the total mean power per non-pilot subcarrier is even higher due to the spread of the pilots according to $\mathbf{G}_p\mathbf{p}$. Within the presented signaling framework, CP-OFDM is modelled by the generator matrices $\mathbf{G}_{d,\text{cp}} = \mathbf{B}_p\mathbf{I}$ and $\mathbf{G}_{p,\text{cp}} = \mathbf{P}_p \begin{bmatrix} \mathbf{I} & \mathbf{0}^T \end{bmatrix}^T$, assuming appropriately sized identity and zero matrices. Burstwise transmission of OFDM symbols is applied, for details on the whole transmission chain (data modulation alphabet, channel encoder, etc.), the interested reader is referred to [29].

Zero additive noise $\mathbf{v}'' = \mathbf{0}$, cf. (26), is assumed throughout this section in order to distinctly elaborate on the degrading effects of a CFO. The results are obtained by averaging over

Table II: Summary of the main PHY parameters of the exemplary UW-OFDM and CP-OFDM setup.

		UW-OFDM	CP-OFDM
DFT size	N	64	64
data subcarriers	N_d, N_d'	32	48
zero subcarriers	N_z	12	12
pilot subcarriers	N_p	4	4
red. subcarriers	N_r	16	-
guard interval samples	N_g, N_u	16	16
zero subcarrier indices	$\mathcal{I}_z$	{0,27,28,…,37}	{0,27,28,…,37}
pilot subcarrier indices	$\mathcal{I}_p$	{7,21,43,57}	{7,21,43,57}
red. subcarrier indices	$\mathcal{I}_r$	{2,5,9,13,17,20,24 26,38,40,44 47,51,54,58,62}	{}
DFT length	T_{DFT}	3.2 μs	3.2 μs
guard interval length	T_{GI}	0.8 μs	0.8 μs
OFDM symbol lengh	T_{OFDM}	3.2 μs	4 μs
subcarrier spacing	Δ_f	312.5 kHz	312.5 kHz

10^4 independent realizations of channel impulse responses with unit energy, drawn from a model with exponentially

decaying power delay profile [44] and assuming a channel delay spread of $\tau_{\text{RMS}} = 100\,\text{ns}$.

The CFO ϵ has been estimated according to (53) once per burst based on the estimated CPE of the first OFDM symbol $\hat{\varphi}_0$. The CPEs $\hat{\varphi}_l$ are estimated according to (23) with $\mathbf{W}_p = |\hat{\mathbf{H}}_p|^2$. The equalizer is the same as for CP-OFDM and has been chosen to be $\mathbf{E}_p = \begin{bmatrix} \mathbf{0} & \mathbf{I} \end{bmatrix} \mathbf{P}_p^T$. Perfect channel knowledge is assumed at the receiver.

B. Simulation Results

Fig. 7 clearly shows that UW-OFDM outperforms CP-OFDM in terms of estimating φ_l based on frequency pilot tones, regardless of the utilized generator matrix and the UW. The performance variation among different UWs is due to
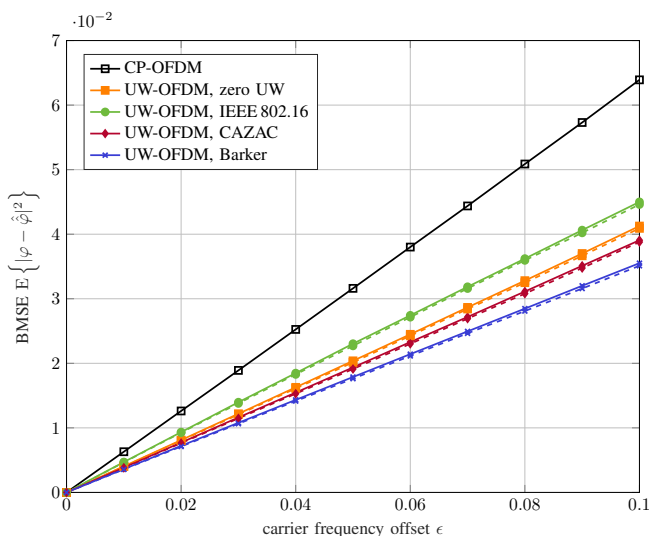

Figure 7: Comparison of estimation error of the CFO induced CPE φ_l between UW-OFDM and CP-OFDM in terms of Bayesian mean square error (BMSE). Investigated scenario: $\mathbf{G}_d'$ (solid line), $\mathbf{G}_d''$ (dashed line), $\mathbf{W}_p = |\tilde{\mathbf{H}}_p|^2$, and a multipath environment with $\tau_{\text{RMS}} = 100\,\text{ns}$.

two reasons. First of all, the approximation of φ_p as an affine function is not equally accurate for all UWs, cf. Fig. 6. Second of all, in some cases (e.g., for a Barker sequence) the portions of the UW overlaying the pilot subcarriers coincidentally add up coherently with the pilot symbols and thus increase the resulting signal-to-interference-noise ratio in the estimation process, cf. (37). The latter is also the reason why a zero UW — contrary to intuitive expectations, as in this case there are no UW induced disturbances — does not deliver the best results. Independent of that, there is a principle performance gap between UW-OFDM and CP-OFDM, regardless of a specific UW design. The reason for this gap becomes immediately apparent when studying all sources degrading $\hat{\hat{\varphi}}_l$, which can be seen from $\hat{p}^{(l)}[k]$ in (30). Therefore, let us evaluate the mean power of the data driven ICI disturbances

$$\sigma_{d_{\text{ICI}}}^2 = \frac{1}{N_p} \sum_{k=0}^{N_p-1} \text{E}\left\{ d_{\text{ICI}}^{(l)}[k] d_{\text{ICI}}^{(l)}[k]^H \right\} \tag{55}$$

$$= \frac{1}{N_p} \sum_{k=0}^{N_p-1} \text{E}\left\{ \mathbf{e}_k^T \tilde{\mathbf{\Lambda}}_h^{(l)} \mathbf{G}_d \mathbf{d}^{(l)} \mathbf{d}^{(l)H} \mathbf{G}_d^H \tilde{\mathbf{\Lambda}}_h^{(l)H} (\mathbf{e}_k^T)^H \right\} \tag{56}$$

$$= \sigma_d^2 \frac{1}{N_p} \sum_{k=0}^{N_p-1} \mathbf{e}_k^T \tilde{\mathbf{\Lambda}}_{h,\text{stat}} \mathbf{G}_d \mathbf{G}_d^H \tilde{\mathbf{\Lambda}}_{h,\text{stat}}^H (\mathbf{e}_k^T)^H, \tag{57}$$

where $\tilde{\mathbf{\Lambda}}_h^{(l)} = \text{e}^{j\varphi_l} \tilde{\mathbf{\Lambda}}_{h,\text{stat}}$ and $d_{\text{ICI}}^{(l)}[k]$ denotes the kth element of the vector $\mathbf{d}_{\text{ICI}}^{(l)}$ given in (27). It turns out that the redundancy introduced by the UW-OFDM generator matrix reduces the resulting interferences significantly, yielding $\sigma_{d_{\text{ICI}},\text{cp}}^2 > \sigma_{d_{\text{ICI}},\text{uw}}^2$ for an increasing CFO as shown in Fig. 8. The mean power
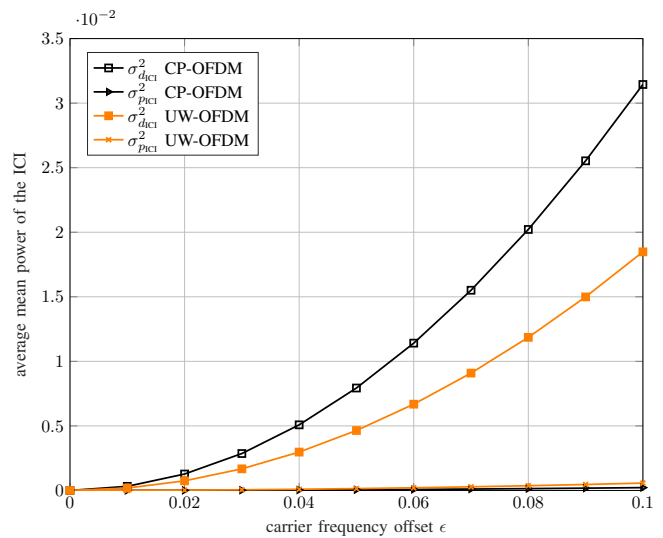

Figure 8: Comparison of the average mean power of the ICI experienced by a pilot symbol in UW-OFDM and CP-OFDM. The ICI is separated into the data part and the part induced by the other pilots. Investigated scenario: $\mathbf{G}_d'$ and a multipath environment with $\tau_{\text{RMS}} = 100\,\text{ns}$.

of the pilot induced ICI

$$\sigma_{p_{\text{ICI}}}^2 = \frac{1}{N_p} \sum_{k=0}^{N_p-1} \text{E}\left\{ p_{\text{ICI}}^{(l)}[k] p_{\text{ICI}}^{(l)}[k]^H \right\} \tag{58}$$

with $p_{\text{ICI}}^{(l)}[k] = \mathbf{e}_k^T \tilde{\mathbf{\Lambda}}_h^{(l)} \sum_{m=0,m\neq k}^{N_p-1} \mathbf{g}_m p[m]$ from (31) is a little bit higher for UW-OFDM, but without any relevance. We conclude that UW-OFDM clearly outperforms CP-OFDM in terms of pilot based estimation of the CFO induced CPE, regardless of the specific setup.

VI. Conclusion

Pilot tones in the frequency domain are a well-established means for estimating various system parameters. This work has provided a framework to include them into UW-OFDM signals. The presented framework allows optimizing an UW-OFDM signal towards two criteria at the same time, to achieve optimum data estimation capabilities on the one hand, as well as the most energy efficient pilot insertion on the other hand. Contrary to conventional OFDM, pilot tone based CPE

estimates incorporate an additional phase offset in case of UW-OFDM, which has to be accounted for. This phase offset depends on the channel instance and the utilized setup. An MSE analysis confirms that the same pilot tone based estimation method provides a significantly better estimate of the CPE in UW-OFDM than in CP-OFDM. This is due the redundancy present in UW-OFDM signals, decreasing the ICI that causes otherwise a degradation of the estimation performance.

APPENDIX A
DERIVATION OF CFO MODEL

In this Appendix we derive a comprehensive CFO signaling model for UW-OFDM[9]. We start with a description of the CFO effects in time domain and finally end up with the model in (19), describing the receive signal of the lth OFDM symbol in the frequency domain.

Assuming a carrier frequency offset f_{CFO} present in a system, the time domain samples in the complex baseband experience an incremental phase shift of

$$y(uT_s) = e^{j2\pi f_{\text{CFO}} uT_s} e^{j\phi_0} x(uT_s), \qquad (59)$$

where u denotes the discrete time variable, T_s the sampling time and ϕ_0 an arbitrary phase offset. Perfect timing synchronization is expected to take care of ϕ_0, hence it is set to $\phi_0 = 0$ and discarded in the following. The impact of f_{CFO} on the OFDM system performance depends on the relative proportion to the subcarrier spacing Δ_f rather than on the absolute value, thus motivating to introduce a relative carrier frequency offset

$$\epsilon = \frac{f_{\text{CFO}}}{\Delta_f} = \frac{f_{\text{CFO}}}{f_s/N} = \frac{f_{\text{CFO}} N}{f_s} = f_{\text{CFO}} NT_s. \qquad (60)$$

With (60) the incremental phase offset in (59) translates to $e^{j\frac{2\pi\epsilon u}{N}}$ (where $u = 0, 1, \ldots N-1$ when considering only one OFDM symbol) and in matrix notation to

$$\mathbf{y} = \mathbf{\Lambda}' \mathbf{x} \qquad (61)$$

with $\mathbf{\Lambda}' \in \mathbb{C}^{N \times N}$ given as $\mathbf{\Lambda}' = \text{diag}\left(\begin{bmatrix} 1 & e^{j\frac{2\pi\epsilon}{N}} & \cdots & e^{j\frac{2\pi\epsilon(N-1)}{N}} \end{bmatrix}^T\right)$. In order to take into account the phase accumulated by previous OFDM symbols and the additional UW in front of the burst (which ensures the cyclic structure for the first OFDM symbol), a diagonal matrix $\mathbf{\Lambda}'^{(l)} \in \mathbb{C}^{N \times N}$ with

$$\mathbf{\Lambda}'^{(l)} = e^{j\psi_l} \mathbf{\Lambda}' = e^{j\frac{2\pi\epsilon(Nl+N_u)}{N}} \mathbf{\Lambda}' \qquad (62)$$

is introduced, whereas $l \in \{0, 1, \ldots L-1\}$, L denotes the number of OFDM symbols per burst, and ψ_l is a phase offset defined as

$$\psi_l = \frac{2\pi\epsilon(Nl + N_u)}{N}. \qquad (63)$$

In the following, matrices with the notation $'$ as e.g., $\mathbf{\Lambda}'$ encompass the whole frequency range including the zero subcarriers. The counterpart $\mathbf{\Lambda}$ and similar matrices introduced later will only comprise non-zero subcarriers.

[9] Note that parts of the CFO model have already been developed in [45].

Starting with the UW-OFDM transmit signal in (10) and taking into account (62), the lth OFDM time domain symbol at the receiver can be modelled as

$$\mathbf{y}_r^{(l)} = \mathbf{\Lambda}'^{(l)} \mathbf{H}_c \mathbf{F}_N^{-1} \left(\mathbf{BG}_d \mathbf{d} + \mathbf{BG}_p \mathbf{p} + \tilde{\mathbf{x}}_u\right) + \mathbf{n} \qquad (64)$$

$$= \mathbf{\Lambda}'^{(l)} \mathbf{F}_N^{-1} \mathbf{F}_N \mathbf{H}_c \mathbf{F}_N^{-1} \left(\tilde{\mathbf{x}}_d^{(l)} + \tilde{\mathbf{x}}_p + \tilde{\mathbf{x}}_u\right) + \mathbf{n} \qquad (65)$$

$$= \mathbf{\Lambda}'^{(l)} \mathbf{F}_N^{-1} \tilde{\mathbf{H}}' \tilde{\mathbf{x}}''^{(l)} + \mathbf{n}, \qquad (66)$$

with $\tilde{\mathbf{x}}''^{(l)} = \tilde{\mathbf{x}}_d^{(l)} + \tilde{\mathbf{x}}_p + \tilde{\mathbf{x}}_u \in \mathbb{C}^{N \times 1}$ summarizing the effects of data, pilots and the UW in one frequency domain vector. Applying the DFT yields the frequency domain OFDM symbol

$$\tilde{\mathbf{y}}_r^{(l)} = \mathbf{F}_N \mathbf{y}_r^{(l)} \qquad (67)$$

$$= \mathbf{F}_N \mathbf{\Lambda}'^{(l)} \mathbf{F}_N^{-1} \tilde{\mathbf{H}}' \tilde{\mathbf{x}}''^{(l)} + \mathbf{F}_N \mathbf{n} \qquad (68)$$

$$= \tilde{\mathbf{\Lambda}}'^{(l)} \tilde{\mathbf{H}}' \tilde{\mathbf{x}}''^{(l)} + \mathbf{v}', \qquad (69)$$

with a noise vector $\mathbf{v}' \in \mathbb{C}^{N \times 1}$ defined as

$$\mathbf{v}' = \mathbf{F}_N \mathbf{n} \sim \mathcal{CN}(\mathbf{0}, N\sigma_n^2 \mathbf{I}). \qquad (70)$$

Since $\mathbf{\Lambda}'^{(l)}$ is diagonal, multiplying with $\mathbf{F}_N$ and $\mathbf{F}_N^{-1}$ results in a circulant matrix $\tilde{\mathbf{\Lambda}}'^{(l)}$. In order to provide a better insight on $\tilde{\mathbf{\Lambda}}'^{(l)}$ and its relationship to ϵ, let us start with the definition of the kth element of vector $\tilde{\mathbf{y}}_r^{(l)}$

$$\tilde{y}_r^{(l)}[k] = [\mathbf{F}_N]_{k,*} \mathbf{y}_r^{(l)} = \sum_{u=0}^{N-1} e^{-j\frac{2\pi ku}{N}} y_r^{(l)}[u]. \qquad (71)$$

According to (66), the uth element of $\mathbf{y}_r^{(l)}$ is expressed as

$$y_r^{(l)}[u] = \left[\mathbf{\Lambda}'^{(l)}\right]_{u,*} \mathbf{F}_N^{-1} \tilde{\mathbf{H}}' \tilde{\mathbf{x}}''^{(l)} + n[u] \qquad (72)$$

$$= e^{j\psi_l} e^{j\frac{2\pi\epsilon u}{N}} \left[\mathbf{F}_N^{-1}\right]_{u,*} \tilde{\mathbf{H}}' \tilde{\mathbf{x}}''^{(l)} + n[u] \qquad (73)$$

$$= e^{j\psi_l} e^{j\frac{2\pi\epsilon u}{N}} \frac{1}{N} \sum_{m=0}^{N-1} e^{j\frac{2\pi mu}{N}} \left[\tilde{\mathbf{H}}'\right]_{m,m} \tilde{x}''^{(l)}[m] + n[u]. \qquad (74)$$

Note that (73) follows from (72) by considering that only the uth element of the vector $\left[\mathbf{\Lambda}'^{(l)}\right]_{u,*}$ is non-zero. Plugging (74) into (71) and rearranging yields

$$\tilde{y}_r^{(l)}[k] = \sum_{u=0}^{N-1} e^{-j\frac{2\pi ku}{N}} e^{j\psi_l} e^{j\frac{2\pi\epsilon u}{N}} \qquad (75)$$

$$\times \frac{1}{N} \sum_{m=0}^{N-1} e^{j\frac{2\pi mu}{N}} \left[\tilde{\mathbf{H}}'\right]_{m,m} \tilde{x}''^{(l)}[m] + v'[k] \qquad (76)$$

$$= e^{j\psi_l} \frac{1}{N} \sum_{u=0}^{N-1} \sum_{m=0}^{N-1} e^{j\frac{2\pi(m+\epsilon-k)u}{N}} \left[\tilde{\mathbf{H}}'\right]_{m,m} \tilde{x}''^{(l)}[m] + v'[k] \qquad (77)$$

$$= e^{j\psi_l} \frac{1}{N} \sum_{m=0}^{N-1} \left[\tilde{\mathbf{H}}'\right]_{m,m} \tilde{x}''^{(l)}[m] \sum_{u=0}^{N-1} e^{j\frac{2\pi(m+\epsilon-k)u}{N}} + v'[k]. \qquad (78)$$

The relationship between $\tilde{\mathbf{y}}_r^{(l)}$ and $\tilde{\mathbf{x}}''^{(l)}$ is fully determined by $\tilde{\mathbf{\Lambda}}'^{(l)} \tilde{\mathbf{H}}'$, cf. (69). Applying this knowledge on (78) together with

$$\tilde{\mathbf{\Lambda}}'^{(l)} = e^{j\psi_l} \tilde{\mathbf{\Lambda}}' \qquad (79)$$

leads to the definition

$$\left[\tilde{\boldsymbol{\Lambda}}'\right]_{k,m} = \frac{1}{N}\sum_{u=0}^{N-1}\mathrm{e}^{j\frac{2\pi}{N}(m+\epsilon-k)u} \qquad k=0\ldots N-1;$$
$$m=0\ldots N-1. \quad (80)$$

These formulas allow a compact notation of $\tilde{\boldsymbol{\Lambda}}'^{(l)}$, however, an immediate interpretation of the CFO impact in the frequency domain is rather difficult. This will thus be provided in the following. Let $\tilde{x}_h^{(l)}[m] = \left[\tilde{\mathbf{H}}'\right]_{m,m}\tilde{x}''^{(l)}[m]$ for reasons of compactness, and separate the impact of the subcarrier in consideration (indicated with index k) from all others, then (78) can be rewritten as

$$\tilde{y}_r^{(l)}[k] = \frac{1}{N}\mathrm{e}^{j\psi_l}\tilde{x}_h^{(l)}[k]\sum_{u=0}^{N-1}\mathrm{e}^{j\frac{2\pi\epsilon u}{N}}$$
$$+ \frac{1}{N}\mathrm{e}^{j\psi_l}\sum_{m=0,m\neq k}^{N-1}\tilde{x}_h^{(l)}[m]\sum_{u=0}^{N-1}\mathrm{e}^{j\frac{2\pi(m+\epsilon-k)u}{N}} + v'[k]$$
$$(81)$$

$$= \frac{1}{N}\mathrm{e}^{j\psi_l}\tilde{x}_h^{(l)}[k]\frac{1-\mathrm{e}^{j2\pi\epsilon}}{1-\mathrm{e}^{j\frac{2\pi\epsilon}{N}}}$$
$$+ \frac{1}{N}\mathrm{e}^{j\psi_l}\sum_{m=0,m\neq k}^{N-1}\tilde{x}_h^{(l)}[m]\frac{1-\mathrm{e}^{j2\pi(m+\epsilon-k)}}{1-\mathrm{e}^{j\frac{2\pi(m+\epsilon-k)}{N}}} + v'[k]$$
$$(82)$$

$$= \frac{1}{N}\mathrm{e}^{j\psi_l}\frac{\mathrm{e}^{j\pi\epsilon}\left(\mathrm{e}^{-j\pi\epsilon}-\mathrm{e}^{j\pi\epsilon}\right)}{\mathrm{e}^{j\frac{\pi\epsilon}{N}}\left(\mathrm{e}^{-j\frac{\pi\epsilon}{N}}-\mathrm{e}^{j\frac{\pi\epsilon}{N}}\right)}\tilde{x}_h^{(l)}[k] + \frac{1}{N}\mathrm{e}^{j\psi_l}$$
$$\times \sum_{m=0,m\neq k}^{N-1}\tilde{x}_h^{(l)}[m]\frac{\mathrm{e}^{j\pi(m+\epsilon-k)}}{\mathrm{e}^{j\frac{\pi(m+\epsilon-k)}{N}}}$$
$$\times \frac{\left(\mathrm{e}^{-j\pi(m+\epsilon-k)}-\mathrm{e}^{j\pi(m+\epsilon-k)}\right)}{\left(\mathrm{e}^{-j\frac{\pi(m+\epsilon-k)}{N}}-\mathrm{e}^{j\frac{\pi(m+\epsilon-k)}{N}}\right)} + v'[k]$$
$$(83)$$

$$= \mathrm{e}^{j\psi_l}\mathrm{e}^{j\frac{\pi\epsilon(N-1)}{N}}\frac{\sin(\pi\epsilon)}{N\sin(\frac{\pi\epsilon}{N})}\tilde{x}_h^{(l)}[k] + \mathrm{e}^{j\psi_l}\mathrm{e}^{j\frac{\pi\epsilon(N-1)}{N}}$$
$$\times \sum_{m=0,m\neq k}^{N-1}\mathrm{e}^{j\frac{\pi(m-k)(N-1)}{N}}\frac{\sin(\pi(m+\epsilon-k))}{N\sin\left(\frac{\pi(m+\epsilon-k)}{N}\right)}\tilde{x}_h^{(l)}[m]$$
$$+ v'[k]. \quad (84)$$

Note that (82) follows from (81) by applying the formula for the sum of a geometric series $S_n = \sum_{p=0}^{P-1} r^p = \frac{1-r^P}{1-r}$, and (83) is a preparation step to apply $\left(\mathrm{e}^{-ja}-\mathrm{e}^{ja}\right)=2j\sin(a)$. Finally, the frequency domain receive signal corrupted by CFO is

$$\tilde{y}_r^{(l)}[k] = \mathrm{e}^{j\psi_l}\mathrm{e}^{j\frac{2\pi}{N}\epsilon\left(\frac{N-1}{2}\right)}\frac{\sin(\pi\epsilon)}{N\sin(\frac{\pi\epsilon}{N})}\left[\tilde{\mathbf{H}}'\right]_{k,k}\tilde{x}''^{(l)}[k]$$
$$+ i^{(l)}[k] + v'[k] \quad (85)$$
$$= \mathrm{e}^{j\varphi_l}\frac{\sin(\pi\epsilon)}{N\sin(\frac{\pi\epsilon}{N})}\left[\tilde{\mathbf{H}}'\right]_{k,k}\tilde{x}''^{(l)}[k] + i^{(l)}[k] + v'[k],$$
$$(86)$$

with an ICI term $i^{(l)}[k]$ given as

$$i^{(l)}[k] = \mathrm{e}^{j\varphi_l}\sum_{m=0,m\neq k}^{N-1}\mathrm{e}^{j\frac{\pi(m-k)(N-1)}{N}}$$
$$\times \frac{\sin(\pi(m+\epsilon-k))}{N\sin\left(\frac{\pi(m+\epsilon-k)}{N}\right)}\left[\tilde{\mathbf{H}}'\right]_{m,m}\tilde{x}''^{(l)}[m],$$
$$(87)$$

and a phase offset

$$\varphi_l = \psi_l + \frac{2\pi}{N}\epsilon\left(\frac{N-1}{2}\right) = \frac{2\pi}{N}\epsilon\left(Nl+N_u+\frac{N-1}{2}\right).$$
$$(88)$$

As can be seen from (86), there are three effects on a subcarrier symbol $\tilde{x}''^{(l)}[k]$ as a result of a CFO:

- A phase offset by φ_l,
- an attenuation by $\frac{\sin(\pi\epsilon)}{N\sin(\pi\epsilon/N)}$, and
- an ICI term $i^{(l)}[k]$ with similar properties as additive noise.

In matrix notation, (86) translates to

$$\tilde{\mathbf{y}}_r^{(l)} = \tilde{\boldsymbol{\Lambda}}'^{(l)}\tilde{\mathbf{H}}'\tilde{\mathbf{x}}''^{(l)} + \mathbf{v}' \quad (89)$$
$$= \mathrm{e}^{j\psi_l}\tilde{\boldsymbol{\Lambda}}'\tilde{\mathbf{H}}'\tilde{\mathbf{x}}''^{(l)} + \mathbf{v}' \quad (90)$$
$$= \mathrm{e}^{j\psi_l}\mathrm{e}^{j\frac{2\pi}{N}\epsilon\left(\frac{N-1}{2}\right)}\tilde{\boldsymbol{\Lambda}}'_{\mathrm{stat}}\tilde{\mathbf{H}}'\tilde{\mathbf{x}}''^{(l)} + \mathbf{v}' \quad (91)$$
$$= \mathrm{e}^{j\varphi_l}\tilde{\boldsymbol{\Lambda}}'_{\mathrm{stat}}\tilde{\mathbf{H}}'\tilde{\mathbf{x}}''^{(l)} + \mathbf{v}', \quad (92)$$

taking into account (79) and

$$\tilde{\boldsymbol{\Lambda}}' = \mathrm{e}^{j\frac{2\pi}{N}\epsilon\left(\frac{N-1}{2}\right)}\tilde{\boldsymbol{\Lambda}}'_{\mathrm{stat}}, \quad (93)$$
$$\left[\tilde{\boldsymbol{\Lambda}}'_{\mathrm{stat}}\right]_{k,m} = \frac{\sin(\pi(m+\epsilon-k))}{N\sin\left(\frac{\pi(m+\epsilon-k)}{N}\right)}\mathrm{e}^{j\frac{\pi(m-k)(N-1)}{N}}. \quad (94)$$

For the main diagonal entries with $k=m$, (94) collapses to $\frac{\sin(\pi\epsilon)}{N\sin(\frac{\pi\epsilon}{N})}$. The nomenclature static within $\tilde{\boldsymbol{\Lambda}}'_{\mathrm{stat}}$ refers to the independence from the OFDM symbol index l.

So far, the derived model is based on $\tilde{\mathbf{y}}_r^{(l)}$ which incorporates all subcarriers. For data estimation performance analysis, it suffices to consider only the subcarriers carrying the payload. We thus discard the zero subcarriers and yield the vector

$$\tilde{\mathbf{y}}_{pl}^{(l)} = \mathbf{B}^T\tilde{\mathbf{y}}_r^{(l)}. \quad (95)$$

Excluding zero subcarriers is straightforward in a CFO free case given in (11) due to the diagonal structure of the channel matrix $\tilde{\mathbf{H}}$. However, $\tilde{\boldsymbol{\Lambda}}'^{(l)}$ in (69) is a dense matrix, hence requiring more in-depth investigations. Conducting a few derivations (for details we refer to [29]), the receive signal in (95) can be expressed as

$$\tilde{\mathbf{y}}_{pl}^{(l)} = \tilde{\boldsymbol{\Lambda}}'^{(l)}\tilde{\mathbf{H}}\mathbf{G}_d\mathbf{d}^{(l)} + \tilde{\boldsymbol{\Lambda}}'^{(l)}\tilde{\mathbf{H}}\mathbf{G}_p\mathbf{p} + \tilde{\boldsymbol{\Lambda}}'^{(l)}\tilde{\mathbf{H}}\mathbf{B}^T\tilde{\mathbf{x}}_u$$
$$+ \tilde{\boldsymbol{\Lambda}}_{zn}^{(l)}\tilde{\mathbf{H}}_z\tilde{\mathbf{x}}_{u,z} + \mathbf{v}. \quad (96)$$

whereas $\mathcal{I}_{nz} = \mathcal{I}_N\backslash\mathcal{I}_z$ denotes the set of non-zero subcarrier indices, $\mathcal{I}_N = \{0,\ldots,N-1\}$, and $\mathcal{I}_z$ represents the positions of zero subcarriers. The offset $\tilde{\boldsymbol{\Lambda}}_{zn}^{(l)}\tilde{\mathbf{H}}_z\tilde{\mathbf{x}}_{u,z}$ with $\left[\tilde{\boldsymbol{\Lambda}}_{zn}^{(l)}\right]_{k,m} = \left[\tilde{\boldsymbol{\Lambda}}'^{(l)}\right]_{\mathcal{I}_{nz}(k),\mathcal{I}_z(m)}$ corresponds to that portion of the UW in frequency domain, which overlays potential zero subcarriers,

i.e., $\tilde{\mathbf{x}}_{u,z}$, and is then spread on <u>n</u>on-zero subcarriers due to ICI. According to Sec. IV-B, we can safely assume that $\tilde{\boldsymbol{\Lambda}}_{zn}^{(l)}\tilde{\mathbf{H}}_z\tilde{\mathbf{x}}_{u,z} \to \mathbf{0}$, yielding the final receive model

$$\tilde{\mathbf{y}}_{pl}^{(l)} \approx \tilde{\boldsymbol{\Lambda}}^{(l)}\tilde{\mathbf{H}}\mathbf{G}_p\mathbf{p} + \tilde{\boldsymbol{\Lambda}}^{(l)}\tilde{\mathbf{H}}\mathbf{G}_d\mathbf{d}^{(l)} + \tilde{\boldsymbol{\Lambda}}^{(l)}\tilde{\mathbf{H}}\mathbf{B}^T\tilde{\mathbf{x}}_u + \mathbf{v} \quad (97)$$

with negligible approximation error.

REFERENCES

[1] M. Huemer, C. Hofbauer, and J. B. Huber, "The Potential of Unique Words in OFDM," in *Proc. 15th Int. OFDM Workshop*, Hamburg, Sep. 2010, pp. 140–144.

[2] M. Huemer, C. Hofbauer, and J. Huber, "Non-Systematic Complex Number RS Coded OFDM by Unique Word Prefix," *IEEE Trans. Signal Process.*, vol. 60, no. 1, pp. 285–299, Jan. 2012.

[3] M. Rajbzadeh, H. Steendam, and H. Khoshbin, "Power Spectrum Characterization of Systematic Coded UW-OFDM Systems," in *Proc. IEEE Veh. Technol. Conf. (VTC Fall)*, Las Vegas, NV, USA, Sep. 2013, p. 5.

[4] M. Rajabzadeh, H. Khoshbin, and H. Steendam, "Sidelobe Suppression for Non-Systematic Coded UW-OFDM in Cognitive Radio Networks," in *Proc. Europ. Wireless Conf.*, Barcelona, Spain, May 2014, pp. 826–831.

[5] M. Rajabzadeh and H. Steendam, "Power Spectral Analysis of UW-OFDM Systems," *IEEE Trans. Commun.*, vol. 66, no. 6, pp. 2685–2695, Jun. 2018.

[6] O. Lang, C. Böck, M. Huemer, and C. Hofbauer, "Increasing the Bandwidth Efficiency in UW-OFDM," in *Proc. Asilomar Conf. Signals, Systems and Computers*, Pacific Grove, CA, USA, Nov. 2019, p. 5.

[7] M. Huemer, A. Onic, and C. Hofbauer, "Linear Data Estimators for UW-OFDM: Classical and Bayesian Approaches," in *Proc. Europ. Signal Proc. Conf. (EUSIPCO)*, Barcelona, Spain, Aug. 2011, pp. 1613–1617.

[8] ——, "Classical and Bayesian Linear Data Estimators for Unique Word OFDM," *IEEE Trans. Signal Process.*, vol. 59, no. 12, pp. 6073–6085, Dec. 2011.

[9] C. Hofbauer and M. Huemer, "A Study of Data Rate Equivalent UW-OFDM and CP-OFDM Concepts," in *Proc. Asilomar Conf. Signals, Systems and Computers*, Pacific Grove, CA, USA, Nov. 2012, pp. 173–177.

[10] M. Huemer, A. Onic, C. Hofbauer, and S. Trampitsch, "Widely Linear Data Estimation for Unique Word OFDM," in *Proc. Asilomar Conf. Signals, Systems and Computers*, Pacific Grove, CA, USA, Nov. 2013, pp. 1934–1938.

[11] C. Hofbauer, C. Böck, and M. Huemer, "From Dedicated Redundant Subcarriers to Distributed Redundancy in UW-OFDM," in *Proc. Asilomar Conf. Signals, Systems and Computers*, Nov. 2016, pp. 1099–1103.

[12] M. Huemer, C. Hofbauer, A. Onic, and J. B. Huber, "On the Exploitation of the Redundant Energy in UW-OFDM: LMMSE Versus Sphere Detection," *IEEE Signal Process. Lett.*, vol. 19, no. 6, pp. 340–343, Jun. 2012.

[13] A. Onic and M. Huemer, "Noise Interpolation for Unique Word OFDM," *IEEE Signal Process. Lett.*, vol. 21, no. 7, pp. 814–818, Jul. 2014.

[14] A. Onic, "Receiver Concepts for Unique Word OFDM," Ph.D. dissertation, Institute of Networked and Embedded Systems, Alpen-Adria-Universität Klagenfurt, Nov. 2013.

[15] W. Haselmayr, C. Hofbauer, B. Etzlinger, A. Springer, and M. Huemer, "Iterative Detection for Unique Word OFDM," in *Proc. Conf. Global Commun. (Globecom)*, Austin, TX, USA, Dec. 2014, pp. 3261–3266.

[16] W. Haselmayr, C. Hofbauer, M. Huemer, and A. Springer, "Approaching the Matched Filter Bound with Unique Word OFDM," in *Proc. IEEE Int. Conf. Commun. (ICC)*, May 2019, pp. 1–4.

[17] C. Douillard, M. Jezequel, C. Berrou, A. Picar, P. Didier, and A. Glavieux, "Iterative Correction of Intersymbol Interference: Turbo Equalization," *Proc. Eur. Trans. Telecommun. (ETT)*, vol. 6, no. 3, pp. 507–511, Sep. 2012.

[18] M. Tuechler, A. C. Singer, and R. Koetter, "Minimum Mean Squared Error Equalization using a Priori Information," *IEEE Trans. Signal Process.*, vol. 50, no. 3, pp. 673–683, Mar. 2002.

[19] D. V. Welden, H. Steendam, and M. Moeneclaey, "Iterative DA/DD Channel Estimation for KSP-OFDM," in *Proc. IEEE Int. Conf. Commun. (ICC)*, Beijing, China, May 2008, pp. 693–697.

[20] "Framing Structure, Channel Coding and Modulation for Digital Television Terrestrial Broadcasting System," Chinese National Standard, Std. GB 20 600-2006, 2006.

[21] C. yen Ong, J. Song, C. Pan, and Y. Li, "Technology and Standards of Digital Television Terrestrial Multimedia Broadcasting [Topics in Wireless Communications]," *IEEE Commun. Mag.*, vol. 48, no. 5, pp. 119–127, May 2010.

[22] S. Tang, F. Yang, K. Peng, C. Pan, K. Gong, and Z. Yang, "Iterative Channel Estimation for Block Transmission with Known Symbol Padding — A New Look at TDS-OFDM," in *Proc. Conf. Global Commun. (Globecom)*, Washington, DC, USA, Nov. 2007, pp. 4269–4273.

[23] M. Muck, M. de Courville, and P. Duhamel, "A Pseudorandom Postfix OFDM Modulator—Semi-Blind Channel Estimation and Equalization," *IEEE Trans. Signal Process.*, vol. 54, no. 3, pp. 1005–1017, Mar. 2006.

[24] L. Jingyi, W. Hai, P. Joo, and J. Ro, "The Effect of Filling Unique Words to Guard Interval for OFDM System," C802.16a-02/87, IEEE 802.16 Broadband Wireless Access Working Group, Sep. 2002.

[25] A. Onic and M. Huemer, "Limiting the Complexity of Sphere Decoding for UW-OFDM," in *Proc. Int. OFDM Workshop*, Hamburg, Sep. 2011, pp. 135–139.

[26] J. B. Huber, J. Rettelbach, M. Seidl, and M. Huemer, "Signal Shaping for Unique-Word OFDM by Selected Mapping," in *Proc. Europ. Wireless Conf.*, Poznan, Poland, Apr. 2012, p. 8.

[27] J. Rettelbach and J. B. Huber, "PMR-Reduction for Continuous Time OFDM Transmit Signals by Selected Mapping," in *Proc. Int. Symp. Signals, Syst. and Electron. (ISSE)*, Potsdam, Germany, Oct. 2012.

[28] F. Classen and H. Meyr, "Frequency Synchronization Algorithms for OFDM Systems Suitable for Communication over Frequency Selective Fading Channels," in *Proc. IEEE Veh. Technol. Conf. (VTC Spring)*, Stockholm, Sweden, Jun. 1994, pp. 1655–1659.

[29] C. Hofbauer, "Design and Analysis of Unique Word OFDM," Ph.D. dissertation, Institute of Networked and Embedded Systems, Alpen-Adria-Universität Klagenfurt, Jun. 2016.

[30] S. Ehsanfar, M. Chafii, and G. Fettweis, "A Frame Design for MIMO UW based Systems: Overhead Analysis & Channel Estimation," in *Proc. 5G World Forum (WF-5G)*, Dresden, Germany, Sep 2019, pp. 1–6.

[31] ——, "A Study on Unique-Word based Synchronization for MIMO Systems over Time-Varying Channels," in *Proc. Wireless Comm. Netw. Conf. (WCNC)*, Seoul, Korea, Apr 2020, pp. 1–7.

[32] C. Hofbauer, W. Haselmayr, and M. Huemer, "Pilot Tone Insertion and Utilization in Unique Word OFDM," in *submitted to Proc. Int. Workshop Signal Proc. Adv. Wireless Comm. (SPAWC)*, Atlanta, GA, USA, May 2020, p. 5.

[33] M. Huemer, C. Hofbauer, A. Onic, and J. B. Huber, "Design and Analysis of UW-OFDM Signals," *Int. J. Electron. and Commun. AEU*, vol. 68, no. 10, pp. 958–968, Oct. 2014.

[34] A. Onic and M. Huemer, "Direct vs. Two-Step Approach for Unique Word Generation in UW-OFDM," in *Proc. 15th Int. OFDM Workshop*, Hamburg, Sep. 2010, pp. 145–149.

[35] X. Cai and G. B. Giannakis, "Error Probability Minimizing Pilots for OFDM with M-PSK Modulation over Rayleigh-Fading Channels," *IEEE Trans. Veh. Technol.*, vol. 53, no. 1, pp. 146–155, Jan. 2004.

[36] B. M. Popovic̀, "Generalized Chirp-Like Polyphase Sequences with Optimum Correlation Properties," *IEEE Trans. Inf. Theory*, vol. 38, no. 4, pp. 1406–1409, Jul. 1992.

[37] S. W. Golomb and R. A. Scholtz, "Generalized Barker Sequences," *IEEE Trans. Inf. Theory*, vol. 11, no. 4, pp. 533–537, Oct. 1965.

[38] "IEEE Std 802.16-2004, Part 16: Air Interface for Fixed Broadband Wireless Access Systems," IEEE, 2004.

[39] K. Shi, E. Serpedin, and P. Ciblat, "Decision-Directed Fine Synchronization in OFDM Systems," *IEEE Trans. Commun.*, vol. 53, no. 3, pp. 408–412, Mar. 2005.

[40] Y.-R. Tsai, X.-S. Li, and C.-Y. Wei, "Data-Carrier Aided Carrier Frequency Offset Estimation for OFDM Systems," in *Proc. IEEE Veh. Technol. Conf. (VTC Spring)*, May 2008, pp. 898–902.

[41] T. Keller, L. Piazzo, P. Mandarini, and L. Hanzo, "Orthogonal Frequency Division Multiplex Synchronization Techniques for Frequency-Selective Fading Channels," *IEEE J. Sel. Areas Commun.*, vol. 19, no. 6, pp. 999–1008, Jun. 2001.

[42] N. Lashkarian and S. Kiaei, "Class of Cyclic-Based Estimators for Frequency-Offset Estimation of OFDM Systems," *IEEE Trans. Commun.*, vol. 48, no. 12, pp. 2139–2149, Dec. 2000.

[43] S. M. Kay, *Fundamentals of Statistical Signal Processing, Volume I: Estimation Theory*, 1st ed. Prentice Hall, Apr. 1993.

[44] J. Fakatselis, *Criteria for 2.4 GHz PHY Comparison of Modulation*, IEEE Document, 1997, p802.11-97/157r1.

[45] R. S. Kanumalli, "Investigation of Carrier Frequency Offset Estimation Techniques for Unique Word (UW) - OFDM Systems," Master's Thesis, Institute of Networked and Embedded Systems, Alpen-Adria-Universität Klagenfurt, Austria, Sep. 2012.